The Astrophysical Journal, 935:51 (24pp), 2022 August 10 https://doi.org/10.3847/1538-4357/ac7c6c

Young, Blue, and Isolated Stellar Systems in the Virgo Cluster. II. A New Class of Stellar System

Michael G. Jones[1], David J. Sand[1], Michele Bellazzini[2], Kristine Spekkens[3,4], Ananthan Karunakaran[4,5], Elizabeth A. K. Adams[6,7], Giuseppina Battaglia[8,9], Giacomo Beccari[10], Paul Bennet[11], John M. Cannon[12], Giovanni Cresci[13], Denija Crnojević[14], Nelson Caldwell[15], Jackson Fuson[12], Puragra Guhathakurta[16], Martha P. Haynes[17], John L. Inoue[12], Laura Magrini[13], Ricardo R. Muñoz[18], Burçin Mutlu-Pakdil[19,20], Anil Seth[21], Jay Strader[22], Elisa Toloba[23], and Dennis Zaritsky[1]

[1] Steward Observatory, University of Arizona, 933 North Cherry Avenue, Rm. N204, Tucson, AZ 85721-0065, USA; jonesmg@arizona.edu
[2] INAF—Osservatorio di Astrofisica e Scienza dello Spazio di Bologna, Via Gobetti 93/3,I-40129 Bologna, Italy
[3] Department of Physics and Space Science, Royal Military College of Canada P.O. Box 17000, Station Forces Kingston, ON K7K 7B4, Canada
[4] Department of Physics, Engineering Physics and Astronomy, Queen's University, Kingston, ON K7L 3N6, Canada
[5] Instituto de Astrofísica de Andalucía (CSIC), Glorieta de la Astronomía, E-18008 Granada, Spain
[6] ASTRON, the Netherlands Institute for Radio Astronomy, Oude Hoogeveesedijk 4,7991 PD Dwingeloo, The Netherlands
[7] Kapteyn Astronomical Institute, PO Box 800, 9700 AV Groningen, The Netherlands
[8] Instituto de Astrofísica de Canarias, Vía Láctea s/n 38205 La Laguna, Spain
[9] Universidad de La Laguna, Avda. Astrofísico Fco. Sánchez, La Laguna, Tenerife E-38205, Spain
[10] European Southern Observatory, Karl-Schwarzschild-Strasse 2, D-85748 Garching bei München, Germany
[11] Space Telescope Science Institute, 3700 San Martin Drive, Baltimore, MD 21218, USA
[12] Department of Physics & Astronomy, Macalester College, 1600 Grand Avenue, Saint Paul, MN 55105, USA
[13] INAF—Osservatorio Astrofisico di Arcetri, Largo E. Fermi 5, I-50125 Firenze, Italy
[14] University of Tampa, 401 West Kennedy Boulevard, Tampa, FL 33606, USA
[15] Center for Astrophysics, Harvard & Smithsonian, 60 Garden Street, Cambridge, MA 02138, USA
[16] UCO/Lick Observatory, University of California Santa Cruz, 1156 High Street, Santa Cruz, CA 95064, USA
[17] Cornell Center for Astrophysics and Planetary Science, Space Sciences Building, Cornell University, Ithaca, NY 14853, USA
[18] Departamento de Astronomía, Universidad de Chile, Camino El Observatorio 1515, Las Condes, Santiago, Chile
[19] Kavli Institute for Cosmological Physics, University of Chicago, Chicago, IL 60637, USA
[20] Department of Astronomy and Astrophysics, University of Chicago, Chicago IL 60637, USA
[21] Department of Physics & Astronomy, University of Utah, Salt Lake City, UT, 84112, USA
[22] Center for Data Intensive and Time Domain Astronomy, Department of Physics and Astronomy, Michigan State University, East Lansing, MI 48824, USA
[23] Department of Physics, University of the Pacific, 3601 Pacific Avenue, Stockton, CA 95211, USA
Received 2022 May 2; revised 2022 June 17; accepted 2022 June 24; published 2022 August 16

Abstract

We discuss five blue stellar systems in the direction of the Virgo cluster, analogous to the enigmatic object SECCO 1 (AGC 226067). These objects were identified based on their optical and UV morphology and followed up with H I observations with the Very Large Array (and Green Bank Telescope), Multi Unit Spectroscopic Explorer (on the Very Large Telescope) optical spectroscopy, and Hubble Space Telescope imaging. These new data indicate that one system is a distant group of galaxies. The remaining four are extremely low mass ($M_* \sim 10^5$ $M_\odot$), are dominated by young blue stars, have highly irregular and clumpy morphologies, are only a few kiloparsecs across, yet host an abundance of metal-rich, $12 + \log(\mathrm{O/H}) > 8.2$, H II regions. These high metallicities indicate that these stellar systems formed from gas stripped from much more massive galaxies. Despite the young age of their stellar populations, only one system is detected in H I, while the remaining three have minimal (if any) gas reservoirs. Furthermore, two systems are surprisingly isolated and have no plausible parent galaxy within $\sim 30'$ ($\sim$140 kpc). Although tidal stripping cannot be conclusively excluded as the formation mechanism of these objects, ram pressure stripping more naturally explains their properties, in particular their isolation, owing to the higher velocities, relative to the parent system, that can be achieved. Therefore, we posit that most of these systems formed from ram-pressure-stripped gas removed from new infalling cluster members and survived in the intracluster medium long enough to become separated from their parent galaxies by hundreds of kiloparsecs and that they thus represent a new type of stellar system.

Unified Astronomy Thesaurus concepts: Low surface brightness galaxies (940); Dwarf galaxies (416); Galaxy interactions (600); Tidal tails (1701); Ram pressure stripped tails (2126); H I line emission (690); Virgo Cluster (1772)

1. Introduction

Systems with exceptionally high gas-to-stellar mass ratios are of particular interest in extragalactic astronomy as they represent one extreme of galaxy formation, namely, some of the lowest-mass objects that succeed in forming stars. Blind radio surveys of neutral hydrogen (H I) have uncovered a plethora of gas-rich systems that have few, or perhaps no, stars (Saul et al. 2012; Adams et al. 2013; Taylor et al. 2013; Cannon et al. 2015). However, distinguishing those that may be genuine extremely low-mass dwarf galaxies from other classes of objects (Cannon et al. 2015), such as tidal debris and high-velocity clouds (Adams et al. 2016), is a

challenging process owing to the faintness of any associated stellar counterpart to these objects (e.g., Janesh et al. 2019), as well as confusion with foreground Milky Way H I emission, which often dominates the velocity range where candidates are expected to be detectable.

However, attempts to distinguish these objects have led to surprising discoveries, most notably SECCO 1 (also called AGC 226067; Adams et al. 2013, 2015; Bellazzini et al. 2015; Sand et al. 2015; Beccari et al. 2017a; Sand et al. 2017; Bellazzini et al. 2018) and AGC 226178 (Cannon et al. 2015; Junais et al. 2021; Jones et al. 2022). These are two young, blue, extremely low-mass ($M_* \sim 10^5\ M_\odot$), gas-rich, metal-rich, actively star-forming stellar systems in the Virgo cluster. AGC 226178 has a gas-to-stellar mass ratio $(1.4M_{\rm HI}/M_*) \sim 1000$, while SECCO 1 has a ratio of ∼150.[24] The properties of both systems imply that they formed via in situ star formation (SF) in gaseous debris stripped from a much larger object. In the case of AGC 226178, the likely parent object has been identified as the nearby galaxy VCC 2034, to which it is connected via a tenuous, low-column-density, 70 kpc long H I bridge (Jones et al. 2022). However, it is unclear whether this gas was stripped by a high-speed tidal encounter, or by ram pressure from the intracluster medium (ICM). In the case of SECCO 1, despite it being relatively close to the Virgo cluster center, it is still sufficiently isolated that its origin is uncertain, and multiple possible parent objects have been suggested (Sand et al. 2017; Bellazzini et al. 2018).

As alluded to by Sand et al. (2017) and Jones et al. (2022), these two objects are not unique but instead appear to be part of a larger population of similar objects in Virgo. SECCO 1 and AGC 226178 were originally identified through their H I line emission, thereby guaranteeing gas richness. However, with the latest and deepest wide-field imaging surveys it is possible to visually identify objects in the Virgo cluster with similar optical and UV properties, though not necessarily equivalently gas-rich.

In this work, we present comprehensive observations of a sample of isolated, blue stellar systems in the Virgo cluster as part of a campaign to understand their physical properties and origins. These additional candidate objects, along with AGC226067/SECCO1 and AGC226178, were followed up with Hubble Space Telescope (HST) F606W and F814W imaging with the Advanced Camera for Surveys (ACS), and H I observations with the Jansky Very Large Array (VLA) and the Green Bank Telescope (GBT). Additional observations with the Multi Unit Spectroscopic Explorer (MUSE) integral-field spectrograph on the Very Large Telescope (VLT), are presented in a companion paper (Bellazzini et al. 2022; hereafter Paper I).

The sample identification is described in Section 2 and their follow-up observations in Section 3. The results, H I and stellar masses, star formation rates (SFRs), and metallicity measurements are presented in Section 4. In Section 5 we search for potential points of origin of these objects, and we discuss potential formation scenarios in Section 6. Finally, in Section 7 and Section 8 we discuss the fate of these objects and future directions of investigation, before drawing our conclusions in Section 9.

We adopt 16.5 Mpc (Mei et al. 2007) as the distance to the Virgo cluster throughout.

2. Target Identification

We performed a visual search for isolated, blue stellar systems, similar in optical appearance to SECCO 1, using the ∼100 deg^2 of Next Generation Virgo cluster Survey (NGVS; Ferrarese et al. 2012) *ugi* imaging of the Virgo cluster, along with Galaxy Evolution Explorer (GALEX; Martin et al. 2005) UV imaging when available. Characteristic systems display an overdensity of compact blue sources with strong associated UV emission. They also lack a diffuse red component typical of Virgo dwarf galaxies, even when they have ongoing SF. Partial results from this search were presented in Sand et al. (2017). In total, five isolated, blue stellar system candidates (or BCs), which we number 1–5, were identified. All five were followed up with observations with the HST, VLA, and MUSE/VLT. The coordinates of these five targets are listed in Table 1, and their locations relative to the Virgo cluster are shown in Figure 1.

Table 1
BC Coordinates and H I Velocities

Object	R.A.	Decl.	$v_{\rm HI}$/km s^{-1}
BC1	12:39:02.0	+12:12:16.7	
BC2[b]	12:44:27.9	+12:37:13.4	
BC3	12:46:42.5	+10:22:04.8	1581
BC4	12:26:25.7	+14:23:12.2	
BC5	12:26:30.9	+15:10:26.2	
SECCO1	12:21:53.9	+13:27:37.0	−142[a]

Notes. Columns: (1) object name; (2 & 3) coordinates (J2000) of the main body of each object; (4) heliocentric velocity of H I emission (Haynes et al. 2011).
[a] Value for the main body from Adams et al. (2015).
[b] BC2 is a spurious object (Section 4.1).

The object we refer to as BC3 is an independent re-identification (based on optical appearance) of the H I-selected object AGC 226178 from the ALFALFA survey (Haynes et al. 2011; Cannon et al. 2015). This object has already been studied in detail (Cannon et al. 2015; Junais et al. 2021; Jones et al. 2022) and is the BC most similar to SECCO 1.

As discussed in the remainder of this paper, we are now confident that four of the five BCs are genuine SECCO 1 analogs.

3. Observations and Reduction

After the initial identification of our target BCs using NGVS and GALEX we had little information about their properties except that they were similar to SECCO 1 in optical appearance (extremely blue, faint, and clumpy) and that their UV emission indicated some recent or ongoing SF. We therefore pursued a three-pronged observational strategy to uncover their nature: 1) HST imaging to better understand their detailed morphology and stellar populations; 2) observations with MUSE/VLT to measure their redshifts via the Hα line and obtain metallicity measurements; 3) VLA D-array and GBT observations to search for any associated H I line emission and quantify their neutral gas content.

3.1. HST Observations

Each of the five candidates was observed with ACS in the F606W and F814W filters as part of program 15183 (PI: D. Sand). Each target was observed for a total of 2120 s and 2180 s in the two filters, respectively, except BC4, which was observed for 2000 s in each filter. DOLPHOT's (Dolphin 2000, 2016) ACS module was used to align the exposures and perform point-source photometry of the resolved stellar population. The dust maps of Schlegel et al. (1998) and $R_{\rm F606W}$

[24] Here a factor of 1.4 is used to account for helium in the gas mass.

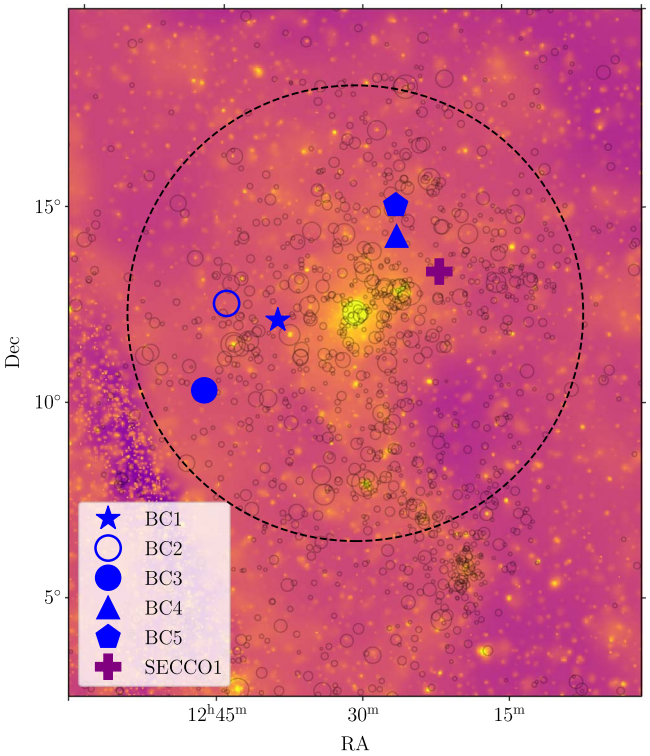

Figure 1. Locations of BCs (and SECCO 1) in the direction of Virgo overlaid on a ROSAT mosaic of hard (0.4–2.4 keV) X-ray emission (Brown et al. 2021). Virgo members and possible members (from the Extended Virgo Cluster Catalog; Kim et al. 2014) are plotted as faint black, unfilled circles. The area of each circle is proportional to the total *r*-band flux of the galaxy it represents. The BCs are shown with blue symbols (see legend) and SECCO 1 is shown as a purple cross. The symbol for BC2 is unfilled as this object is spurious (see Section 4.1). The approximate virial radius (taken to be 1.7 Mpc; Kashibadze et al. 2020) of the cluster is shown by a large dashed black circle.

and $R_{\rm F814W}$ values of Schlafly & Finkbeiner (2011) were used to correct for Galactic extinction at the position of each source. Stars were selected from the resulting DOLPHOT catalog following a similar approach to Jones et al. (2022). Briefly, we select all point-like (type 1 and 2) objects with no photometry flags from the DOLPHOT source catalog. We removed sources with greater than 1 mag of crowding (combined, from the two filters). Finally, the combined (in quadrature) absolute sharpness value was enforced to be below $\sqrt{0.075}$, and a roundness threshold of less than 1 (in both filters) was set. Completeness limits were also estimated as in Jones et al. (2022), based on artificial stars added evenly over both images in each field. The measured 90% completeness limits were fit with the combination of a horizontal line and a one-sided parabola (e.g., Figure 2, bottom panels), and the 50% limits were fit with straight lines.

In addition to the point-source photometry in Section 4.6 we also perform aperture photometry on the combined, drizzled images in each band to measure the integrated magnitudes and colors of the systems. This was performed using the Astropy package Photutils (Bradley et al. 2020) and a combination of manually constructed circular and elliptical apertures enclosing the various clumps of each source. In each case the sky background was subtracted based on the median value within an annulus (circular or elliptical) surrounding the aperture.

3.2. MUSE/VLT Observations

To robustly identify H II regions, obtain optical redshifts and basic kinematics, and measure metallicities, we observed all BCs with MUSE/VLT (Bacon et al. 2014). These observations were carried out as part of program 0101.B-0376A (P.I: R. Mu, noz). They covered the spectral range 4650–9300 Å and a $\simeq 1\farcm0 \times 1\farcm0$ field centered on each target. These observations are discussed in detail in Paper I, and here we present an outline of the data reduction process.

The reduction and analysis of these data followed Beccari et al. (2017a). The individual dithered exposures were calibrated separately and then combined into a single stacked data cube for each target. Hα (and integrated light) peaks at least 3σ above the background were identified using Sextractor (Bertin & Arnouts 1996). The flux of each of these detected sources was measured using a $1\farcs5$ (radius) aperture and a 1D spectrum (with a step size of 1.25 Å) of each source was produced.

Redshifts were measured for all detected Hα clumps, and line fluxes for Hβ, [NII], and [OIII] were measured wherever possible (Tables 2 & 3 of (Paper I)). In Section 4.2 we summarize the findings of these measurements and their implications for the origins of BCs.

3.3. GALEX Data

We searched for archival NUV and FUV data from GALEX at the location of each BC (and SECCO 1). Most of the BCs are within the footprint of the GALEX Ultraviolet Virgo Cluster Survey (GUViCS; Boselli et al. 2011); however, these are not always the deepest data available. For BCs 2, 3, 4 and SECCO 1 we use tiles from GUViCS (typically ∼1.6 ks in both bands), but no FUV data are available for either BC4 or SECCO 1. For BC1 we use tiles "Virgo_Epoque_MOS05" (∼16 ks) and "NGA_Virgo_MOS04" (∼1.6 ks) for NUV and FUV, respectively. For BC5 we use tiles "NGA_NGC4421" (∼2 ks) and "GI1_079012_Group5" (∼1.6 ks).

In Section 4.5 we perform aperture photometry on these GALEX tiles and estimate the SFR in each object. The flux within each aperture was measured from the corresponding background subtracted GALEX tile. Uncertainties were estimated by placing 10,000 circular apertures (equal in area to the target apertures) randomly across the GALEX tile after masking the brightest 1% of pixels. Magnitudes were calculated following the conversions of Morrissey et al. (2007) and extinction corrections used $R_{\rm NUV} = 8.20$ and $R_{\rm FUV} = 8.24$ (Wyder et al. 2007). Finally, these magnitude measurements were converted to SFRs following Iglesias-Páramo et al. (2006), using 4.74 as the bolometric solar absolute magnitude.

3.4. VLA Observations

BC3 was observed previously as part of the ALFALFA "Almost Dark" galaxies sample (VLA program 13A-028, PI: J. Cannon; Cannon et al. 2015). These data were obtained in D-configuration and have a channel width of 7.81 kHz (∼1.65 km s^{-1}), a total bandwidth of 8 MHz, and a total on-source integration time of approximately 1.6 h. These data were re-reduced by Jones et al. (2022) using standard reduction methods in the Common Astronomy Software Applications package (CASA; McMullin et al. 2007). The final imaging used Brigg's robust = 0.5 weighting to provide a compromise between sensitivity and angular resolution for the detected H I emission. The channels were averaged and rebinned to a velocity resolution of 5 km s^{-1}.

The remaining four candidates were observed in the VLA program 18A-185 (PI: K. Spekkens). Each target was observed

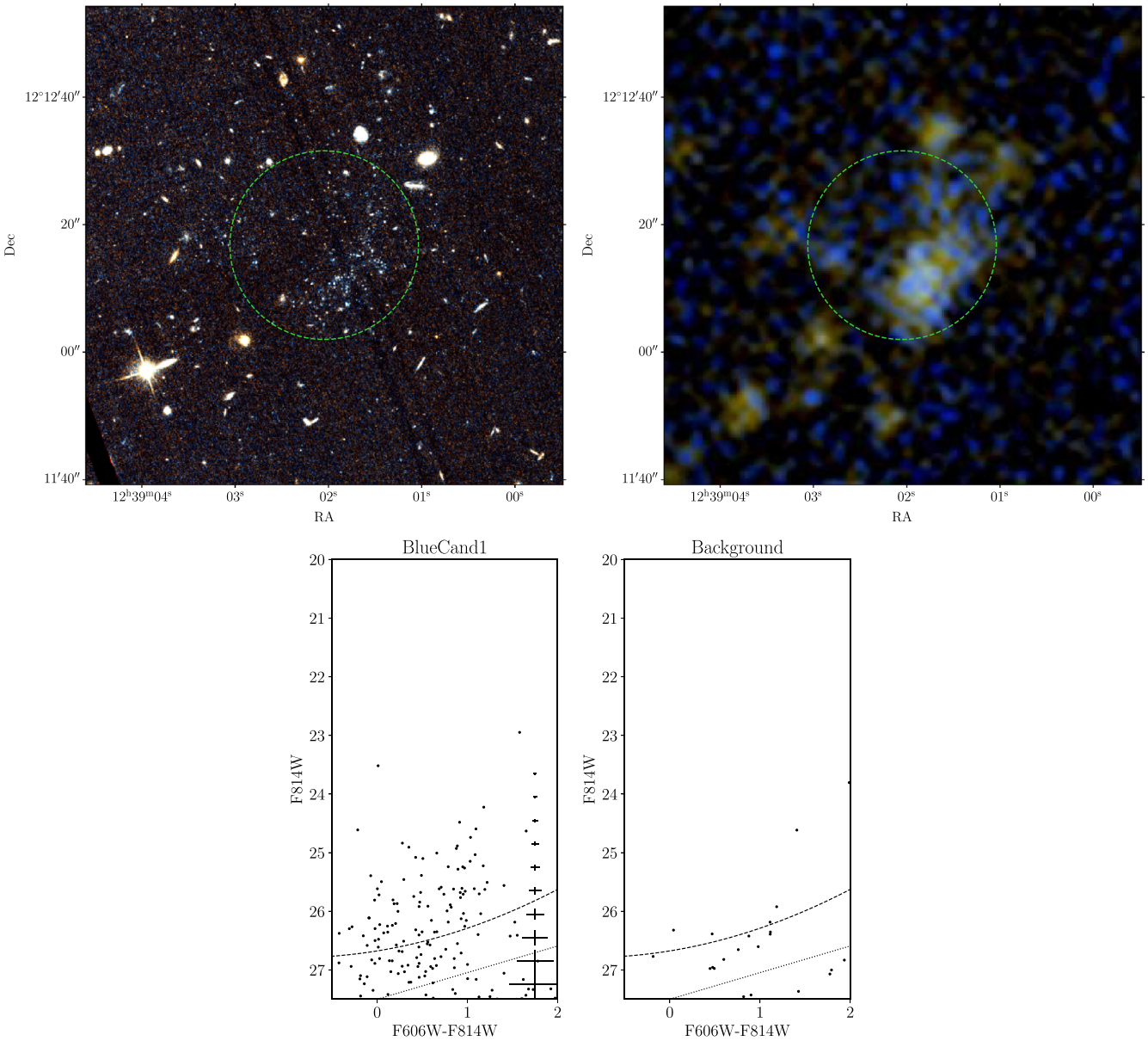

Figure 2. Top left: False color HST F606W+F814W image of BC1. The dashed green circle shows the region used to construct the CMD. At the distance of the Virgo cluster (16.5 Mpc) 20″ is 1.6 kpc. Top right: GALEX NUV+FUV image showing the same field. Bottom left: CMD of the point sources within the aperture shown. The dashed line indicates the 90% completeness limit and the dotted line the 50% limit. The error bars indicate the typical uncertainties (from artificial star tests) in the F814W magnitude and F606W-F814W color as a function of the F814W magnitude. Bottom right: The CMD of a background region of the HST image away from bright sources. The aperture used was equal in area to the target aperture.

on-source for approximately 1.5 hr in D-configuration. The initial observations of both BC1 and BC2 suffered from severe interference and were subsequently reobserved, greatly improving the data quality. As the redshifts of the objects were not known prior to the observations, we used a 32 MHz bandwidth (from 1394.416 to 1426.416 MHz, or approximately -1250 to 5500 km s^{-1}) to search for any H I emission associated with the optical candidates. This range was split up into 3072 channels of 10.42 kHz ($\sim$2.2 km s^{-1}), which during the data reduction was averaged over four channels resulting in a velocity resolution of 8.8 km s^{-1}.

Initially the entire bandwidth of the data was reduced to search for H I emission. However, after the redshifts for all candidates were obtained from MUSE spectroscopy with the VLT, a narrow subband was re-reduced (spanning $\sim$1000 km s^{-1}), allowing for improved local continuum subtraction. The reduction was performed with a `Python` and `CASA`-based pipeline that will be presented in full in Jones et al. (in prep.). The most severe interference was flagged manually and the `tfcrop` flagging algorithm was run in addition. For BC1 we also used `rflag`, after initial calibrations, as there were no bright lines that might be mistaken for interference (other than Milky Way emission). Imaging used Brigg's robust = 2 weighting in order to maximize our detection capabilities. Refer to Table 2 for details of the beam sizes and rms noise for each observation.

3.5. GBT Observations

The large surface area and low system temperature of the GBT allow it to obtain much deeper H I spectra than the VLA, providing a more stringent constraint on any neutral gas content. However, after the redshifts of the candidates were

Table 2
VLA Data Summary

Object	Beam Size	$\sigma_{\rm rms}$/mJy beam^{-1}	$\Delta v_{\rm chan}$/ km s^{-1}
BC1	60″×51″	1.9	8.8
BC2	63″×55″	1.1	8.8
BC3	56″×45″	1.2	5
BC4	65″×54″	0.9	8.8
BC5	65″×54″	1.0	8.8

Note. Columns: (1) object name; (2) synthesized beam size; (3) rms noise; (4) velocity resolution.

known (from their Hα emission), it was determined that only BC1 was suitable for single-dish follow-up, as BC4 and BC5 would be confused with Milky Way emission, BC3 had already been strongly detected with the VLA (Cannon et al. 2015), and the HST imaging of BC2 indicated that it was a background galaxy group (Section 4.1). A director's discretionary time proposal (21A-433, PI: M. Jones) was submitted to the GBT and BC1 was observed for a total of 3 h using ON − OFF position switching. The data were reduced using standard GBT `IDL` procedures. The resulting spectrum has an rms noise of 0.25 mJy (within ± 300 km s^{-1} of the redshift of BC1) after smoothing to a velocity resolution of 30 km s^{-1}.

4. Results

In this section we present the results of our multiwavelength investigation of BCs, providing a description of their morphology, colors, redshifts, stellar masses, metallicities, and gas content. These physical properties will then be used as the basis for a search for candidate parent objects in the following section and a discussion of potential formation pathways in Section 6.

We include SECCO 1 in this sample throughout and either use quantities measured in previous work or (re)measure them as needed (e.g., to provide equivalent values across the whole sample).

4.1. Morphology and Location

The HST images of the BCs are shown in Figures 2, 3, 4, 5, 6, while that for SECCO 1 can be found in Sand et al. (2017). In all cases, except BC2, the BCs appear to be very blue, highly irregular, and frequently broken up into multiple components. Their stellar populations also appear to be partially resolved with some individual stars discernible. These are almost exclusively blue and likely only represent the youngest, brightest stars, not the underlying stellar population. However, their extremely blue appearance (discussed further in Section 4.4 and Section 4.6) also suggests that any redder, underlying population is likely minimal.

The largest single component of any BC is BC3a (Figure 4, top left), which is approximately 30″ across its major axis (2.4 kpc at the distance of Virgo). However, what constitutes a single component is quite subjective; for example, BC4a, b, and c could justifiably be considered as a single object (Paper I). The smallest components (e.g., BC3c, BC5b, BC5c) are less than 5″ (∼400 pc) across and may only consist of a single cluster of stars.

The six components of BC4 are spread over ∼1.′5 (∼7 kpc) and may indicate that this is either a very young collection of objects formed in a gas-rich stream or a somewhat older object that has become gravitationally unbound. Even for the other BCs, which are mostly defined by one or two components, their highly irregular and clumpy structure points to them being extremely low-mass and potentially unbound. Although the individual components of the BCs were identified visually, based primarily on the HST images, nearly all of these clumps have corresponding UV and (usually) Hα emission (Paper I), which indicate ongoing SF. In the case of the latter, the components are all kinematically associated (see Section 4.2).

In the case of BC2, the HST image (Figure 3, top left) is quite distinct from the other BCs and indicates that this is a spurious candidate. It appears to be a distant background group of galaxies rather than a nearby young object. Unlike the other BCs, there is also minimal UV emission (particularly FUV) associated with this candidate (Figure 3, top right), and it was undetected in Hα by MUSE (Section 4.2). Furthermore, almost no stars were identified in its CMD (Figure 3, bottom left), which is consistent with the background (Figure 3, bottom right). Henceforth, we will not regard BC2 as a genuine blue stellar system, and statements regarding the global properties of BCs should be assumed to include SECCO 1, but not BC2.

Figure 1 shows the locations of the BCs in the sky in relation to Virgo cluster galaxies and the cluster virial radius. BC2 is shown as an unfilled symbol. All of the BCs are within the virial radius of the cluster. However, none are in the very cluster center, within ∼2° (∼575 kpc) of M 87 (the central galaxy in the Virgo cluster; Figure 1). BC1 is the closest, with a projected separation of approximately 600 kpc. This may indicate that the parent objects of BCs are recent additions to the cluster.

4.2. Hα Velocities and Metallicities

MUSE detected Hα emission in all BCs, identifying between 4 and 18 distinct clumps of emission in each object (Paper I). The mean velocity (and standard deviation) of these clumps in each source is shown in Table 3. Only BC3 (and SECCO 1) has a prior velocity from an H I detection (Table 1), which matches closely with the Hα velocity for that object. All the objects have velocities that are consistent with Virgo cluster membership ($-500 < cz_{\odot}/{\rm km\,s^{-1}} < 3000$; e.g., Mei et al. 2007), and all are (projected) within the virial radius of the cluster (Figure 1). We note that although BC4, BC5, and SECCO 1 all have negative radial velocities, they are in the vicinity of M 86 ($cz_{\odot} = -224$ km s^{-1}), a region of the Virgo cluster where negative radial velocities are common.

As described in Paper I, the average oxygen abundance of each BC was estimated based on N2 and O3N2 (following Pettini & Pagel 2004), which were corrected for extinction based on the relative strengths of Hα and Hβ. The resulting metallicity estimates are shown in Table 3. All the BCs are extremely high metallicity given their very low stellar masses (Section 4.4), which suggests that they formed from gas pre-enriched in more massive objects. Of particular note are BC4 and 5, both of which are found to be marginally supersolar in metallicity ($12 + \log({\rm O/H})_{\odot} = 8.69$; Asplund et al. 2009). The details of the kinematics and metallicity spreads of the clumps within the BCs are discussed in Paper I.

4.3. H I Mass & Limits

SECCO 1 is the prototype BC, first detected via its H I emission (Adams et al. 2013), having a total H I mass of 1.5×10^7 $M_{\odot}$(Adams et al. 2015). The low resolution of H I observations means that the main and secondary body of

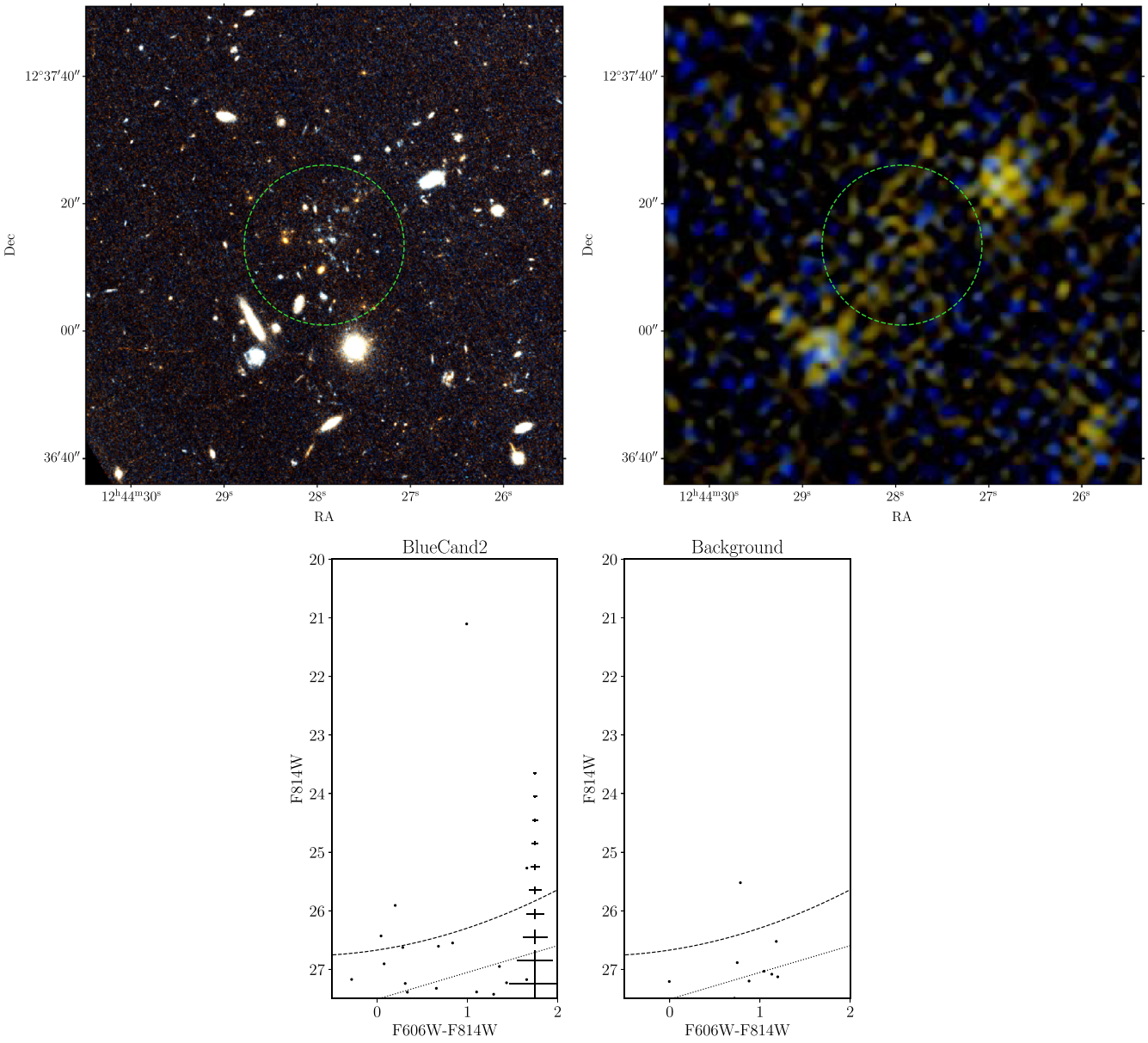

Figure 3. Top left: False color HST F606W+F814W image of BC2. The dashed green circle shows the region used to construct the CMD. Unlike the other BCs, this HST image appears to indicate that this is a background galaxy group. Top right: GALEX NUV+FUV image showing the same field. There is only very weak NUV emission associated with BC2. Bottom: CMD within the aperture shown (left) and a blank field aperture (right). The dotted and dashed lines and error bars are the same as those described in Figure 2, bottom panels. This CMD appears to be consistent with the background, supporting the conclusion that this is a spurious blue stellar system candidate.

SECCO 1 appear as one source in H I. However, Adams et al. (2015) also identified an additional H I-only component slightly to the north as well as another potential optical component, also to the north, but not coincident with any H I. Owing to the similar optical/UV appearance of BCs 1–5 it was anticipated that they would also be H I-rich, which motivated our VLA follow-up program.

In Figures 7, 8, and 9 we present the VLA (and GBT) H I spectra of BCs 1, 3, 4, and 5 (the spectrum of BC2 is discussed in Appendix A). The VLA H I spectra were extracted from the data cubes using an aperture equal to the synthesized beam size, centered on the location of the main body of each BC (Table 1). In addition to these spectra, the data cubes were visually inspected channel by channel, and `SoFiA` was run to search for significant emission features that might be extended spatially or spectrally.

Like SECCO 1, BC3 was known a priori to contain a significant H I reservoir as it was originally identified in the ALFALFA survey (Haynes et al. 2011). However, among BCs 1–5 this is the only object that was detected in our VLA observations. Based on the VLA spectrum (Figure 8; extracted using the `SoFiA` source mask), and an assumed distance of 16.5 Mpc, BC3 has an H I mass of $\log M_{\rm HI}/{\rm M}_{\odot} = 7.3$. This value is 0.3 dex lower than that measured by ALFALFA (Haynes et al. 2011) suggesting that the VLA has not recovered all the extended flux (this was also noted by Cannon et al. 2015; Jones et al. 2022). Jones et al. (2022) show that when viewed in the ALFALFA data cube (which has better column

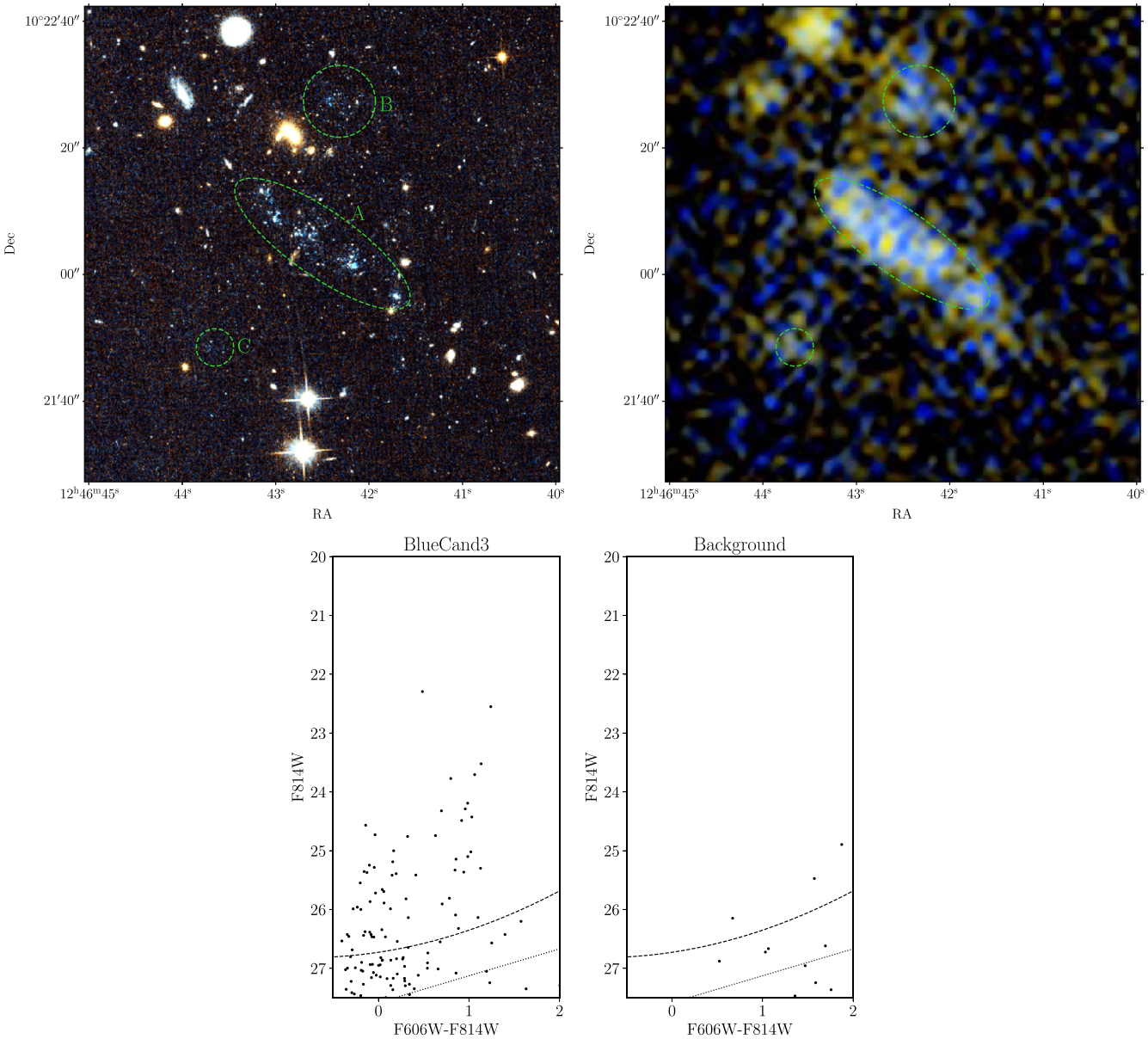

Figure 4. Top left: False color HST F606W+F814W image of BC3. The dashed green ellipse and circles show the regions used to construct the CMD. Top right: GALEX NUV+FUV image showing the same field. Bottom: CMD within the apertures shown (left) and a blank field aperture (right). See Figure 2 caption for further details.

density sensitivity for extended emission than the VLA observations) the H I emission coincident with BC3 appears to connect to the galaxy VCC 2034, approximately 70 kpc to the SW. This galaxy is almost certainly the source of the gas that formed BC3 (discussed further in Section 5, and Jones et al. 2022).

If the other BCs had comparable H I masses to BC3 and SECCO 1, then they would be detected with the VLA observations, but none were (Figures 7 and 9). The slight caveat is that, because of their low radial velocities, BC4 and BC5 might be blended with MW H I emission. The spectrum of BC5 (Figure 9, bottom) also appears to have a peak coincident with the Hα velocity of BC5. However, this peak is below 3σ and extremely narrow, and is likely a noise spike.

All the BCs that are undetected in H I have optical redshift measurements from MUSE Hα observations (BC3 and SECCO 1 do also), and the available H I data can therefore be used with confidence to set upper limits on their H I masses. For BC4 and BC5 the deepest data are those from the VLA, which have rms noise values of 0.9 and 1.0 mJy/beam (at 8.8 km s^{-1} resolution), respectively, at the velocities of the Hα emission. Assuming that any H I emission would fit within one synthesized beam (Table 2) and would have a velocity width of 30 km s^{-1}, then these equate to 3σ upper limits of $\log M_{\rm HI}/{\rm M}_{\odot} < 6.46$ and 6.51, respectively, assuming a fiducial distance of 16.5 Mpc in both cases. For BC1 the GBT follow-up spectrum is by far the more sensitive. With an rms of 0.28 mJy (at 30 km s^{-1} resolution) this gives the 3σ upper limit as $\log M_{\rm HI}/{\rm M}_{\odot} < 6.2$, again assuming a fiducial distance of 16.5 Mpc. These limits are listed in Table 4.

4.4. Stellar Populations

The HST (and GALEX) images and associated CMDs for all BCs are shown in Figures 2, 3, 4, 5, and 6. The blue optical

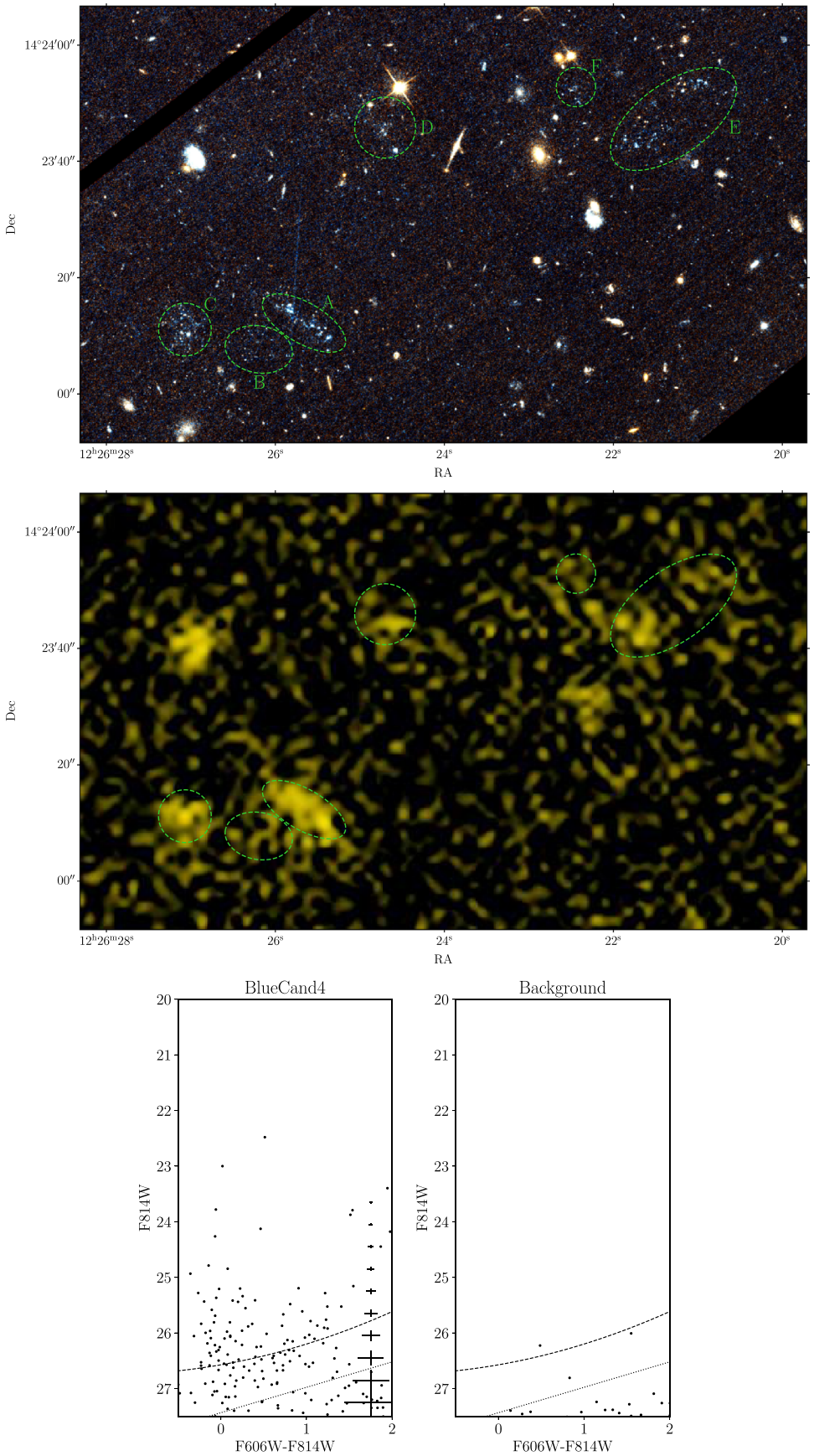

Figure 5. Top: False color HST F606W+F814W image of BC4. The dashed green ellipses and circles show the regions used to construct the CMD. *Middle*: GALEX NUV image showing the same field. Bottom: CMD within the apertures shown (left) and a blank field aperture (right). See Figure 2 caption for further details.

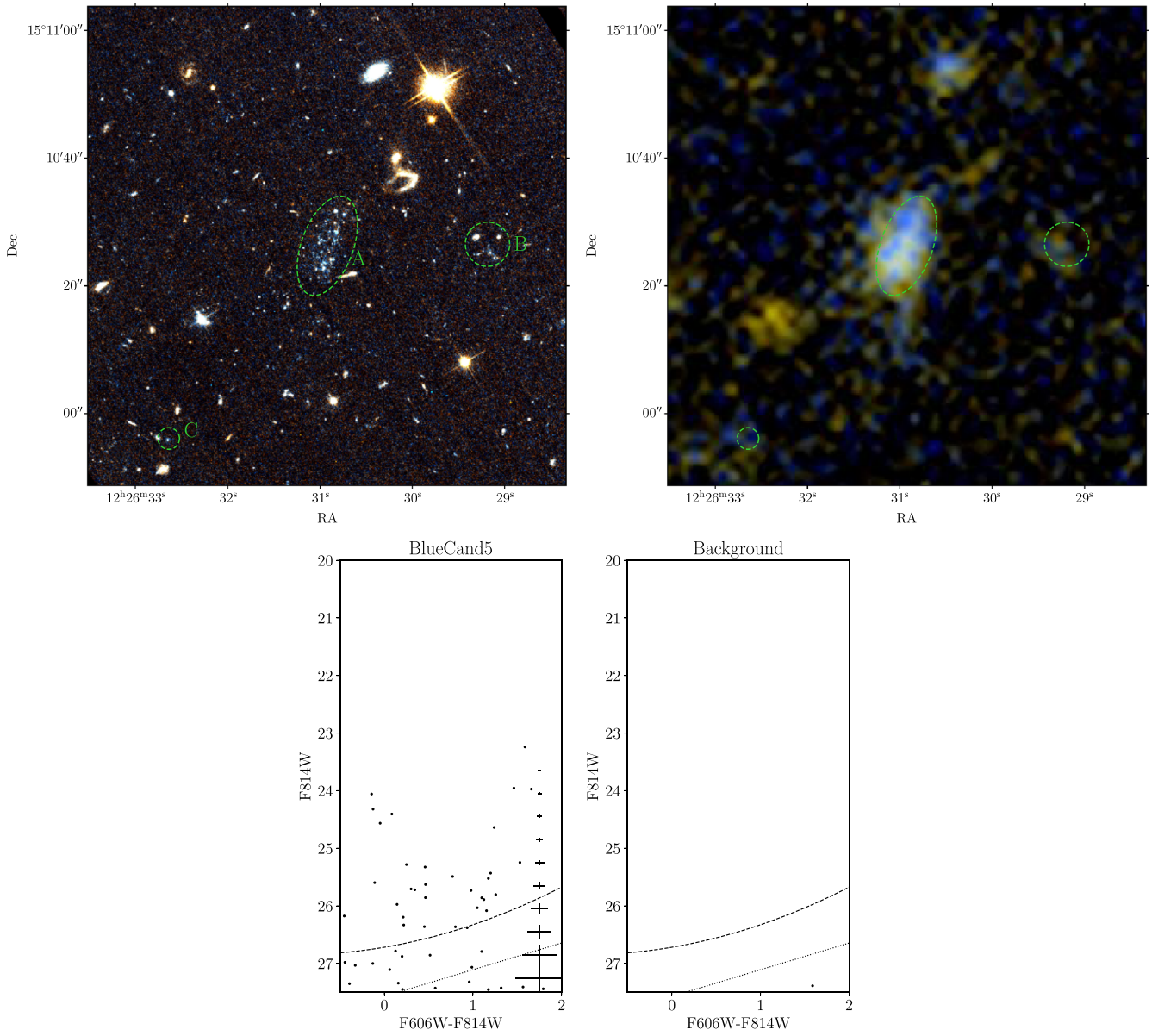

Figure 6. Top left: False color HST F606W+F814W image of BC5. The dashed green ellipse and circle show the regions used to construct the CMD. The component BC5c was identified via Hα emission (Paper I) to be at the same velocity as the main body but may only be a single cluster of stars. Top right: GALEX NUV+FUV image showing the same field. *Bottom*: CMD within the apertures shown (left) and a blank field aperture (right). See Figure 2 caption for further details.

Table 3
Metallicities of BCs

Object	$v_{\mathrm{H}\alpha}$/km s^{-1}	$N_{\mathrm{H}\alpha}$	$N_{\mathrm{O/H}}$	$\langle 12 + \log \mathrm{O/H} \rangle$
BC1	1117 ± 6	18	2	8.35 ± 0.15
BC3	1584 ± 4	15	5	8.29 ± 0.17
BC4	-60 ± 19	16	6	8.73 ± 0.15
BC5	-74 ± 5	4	2	8.70 ± 0.14
SECCO1[a]	-153.2 ± 1.4	33	9	8.38 ± 0.11

Notes. Hα redshift and metallicity measurements from Paper I. Columns: (1) object name; (2) mean velocity (and standard deviation) of Hα clumps detected with MUSE; (3) number of clumps detected in Hα; (4) number of clumps detected in Hα, Hβ, [NII], and [OIII] (suitable for deriving an O/H estimate); (5) mean oxygen abundance and uncertainties (standard deviation of clumps and scatter in O3N2 calibration, 0.14 dex).
[a] Values from Beccari et al. (2017a).

colors and UV emission indicate that the BCs have predominantly young, blue stellar populations. Furthermore, the detection of Hα in all BCs indicates that the youngest stars must be $\leqslant$10 Myr old.

As discussed by Jones et al. (2022), the CMD of BC3 (Figure 4, bottom) is most similar to that of SECCO 1 (Sand et al. 2017), apparently made up almost entirely of blue main-sequence (MS) and helium-burning stars (F814W $\gtrsim$24.5, F606W-F814W $\lesssim$ 0) and red helium-burning (RHeB) stars (23.5 $\lesssim$ F814W $\lesssim$26.5 and F606W-F814W $\gtrsim$ 0.6 mag), with almost no candidates for red giant branch (RGB) stars, highlighting the young age of the population.

BC1's CMD (Figure 2, bottom) is similar, but the brightest RHeB stars are more numerous and fainter than in BC3. These slight differences likely indicate that BC1 is somewhat older

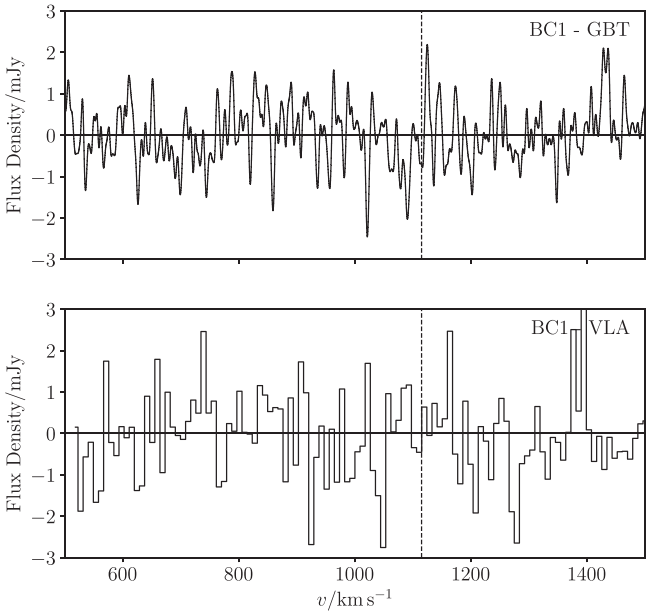

Figure 7. H I spectra of BC1 from the GBT (top) and the VLA (bottom). The VLA spectrum was extracted using an aperture equal in area to the synthesized beam. The vertical dashed lines correspond to the Hα velocity measurement from MUSE. No significant signal is detected in either spectrum.

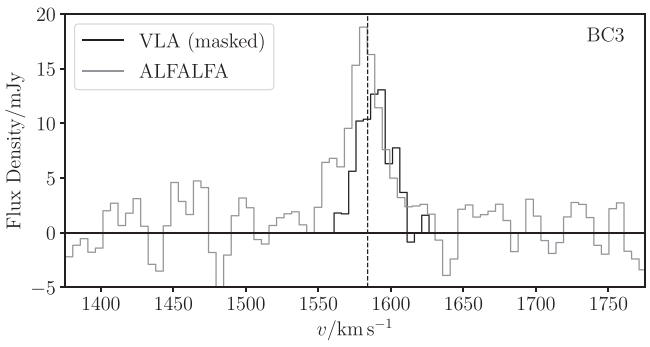

Figure 8. H I spectra of BC3 from ALFALFA and the VLA. The ALFALFA spectrum is the public spectrum from Haynes et al. (2018), and the VLA spectrum was created using the extended source mask of Jones et al. (2022). The vertical dashed line corresponds to the Hα velocity measurement from MUSE. BC3 is detected at a high signal-to-noise ratio in both spectra and both agree with the Hα velocity. However, the VLA measures a somewhat lower flux, with most of the missing emission lying on the approaching side of the line profile. This likely indicates the presence of extended emission below the surface brightness limit of the VLA observations (Cannon et al. 2015; Jones et al. 2022).

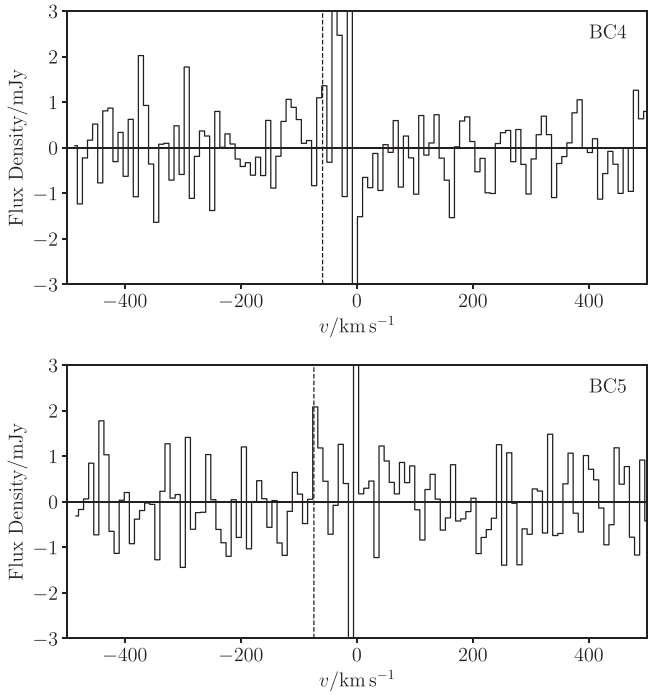

Figure 9. H I spectra in the directions of BC4 (top) and BC5 (bottom) extracted from the VLA H I data cubes within an aperture equal in area to the synthesized beam. The vertical dashed lines correspond to the Hα velocity measurements from MUSE. Neither shows a significant H I line signal, although they could be contaminated with Milky Way H I emission. The apparent peak coincident with the Hα velocity of BC5 is below 3σ and is likely a noise spike.

Table 4
H I Masses of BCs

Object	$M_{\rm HI}/{\rm M}_\odot$	Telescope
BC1	$< 1.6 \times 10^6$	GBT
BC3	4.0×10^7	Arecibo[a]
BC4	$< 2.9 \times 10^6$	VLA
BC5	$< 3.2 \times 10^6$	VLA
SECCO1	1.5×10^7	Arecibo[b]

Notes. Columns: (1) object name; (2) H I mass or 3σ upper limit; (3) telescope for the stated value.
[a] Haynes et al. (2011).
[b] Adams et al. (2015).

than BC3 (as RHeB peak brightness is a function of age; e.g., McQuinn et al. 2011), which would be consistent with its nondetection in H I, if sufficient time has passed for its neutral gas to have been evaporated or stripped.

The CMDs of BC4 and BC5 (Figures 5 and 6, bottom panels) are again similar, but the RHeB stars are even fainter and continue to the completeness limit. This likely indicates that BC4 and BC5 are the oldest objects in the sample. The color spread between the blue and RHeB stars is also wider for BC4 and BC5 than for any of the other BCs.

In Figure 10 we overplot PARSEC isochrones (PAdova and TRieste Stellar Evolution Code; Bressan et al. 2012) on the CMDs of each object for a variety of stellar population ages. As pointed out by Jones et al. (2022), the faintest RHeB stars in BC3 appear consistent with the 50 Myr isochrone, likely indicating that the stellar population in this object cannot be much older than 50 Myr. In the case of the other BCs, as mentioned above, their CMDs imply that their oldest stars are somewhat older (although they must still have formed young stars within the past 10 Myr, as they contain H II regions), but the proximity of the RHeB stars to the completeness limit prevents them from being used to estimate ages. The isochrones also explain the different color gap between the bluest and reddest stars in the CMDs of BC4 and BC5 versus BC1 and BC3. This spread is approximately reproduced in the isochrones and is a function of the higher metallicity of these two objects, which despite their feeble appearance is marginally supersolar (Table 3).

The CMD of SECCO 1 was presented and discussed in Sand et al. (2017) and Bellazzini et al. (2018). The general appearance is similar to the other BCs. The spread between the reddest and bluest stars is most similar to BC1 and BC3, again a reflection of the similar metallicities of these objects.

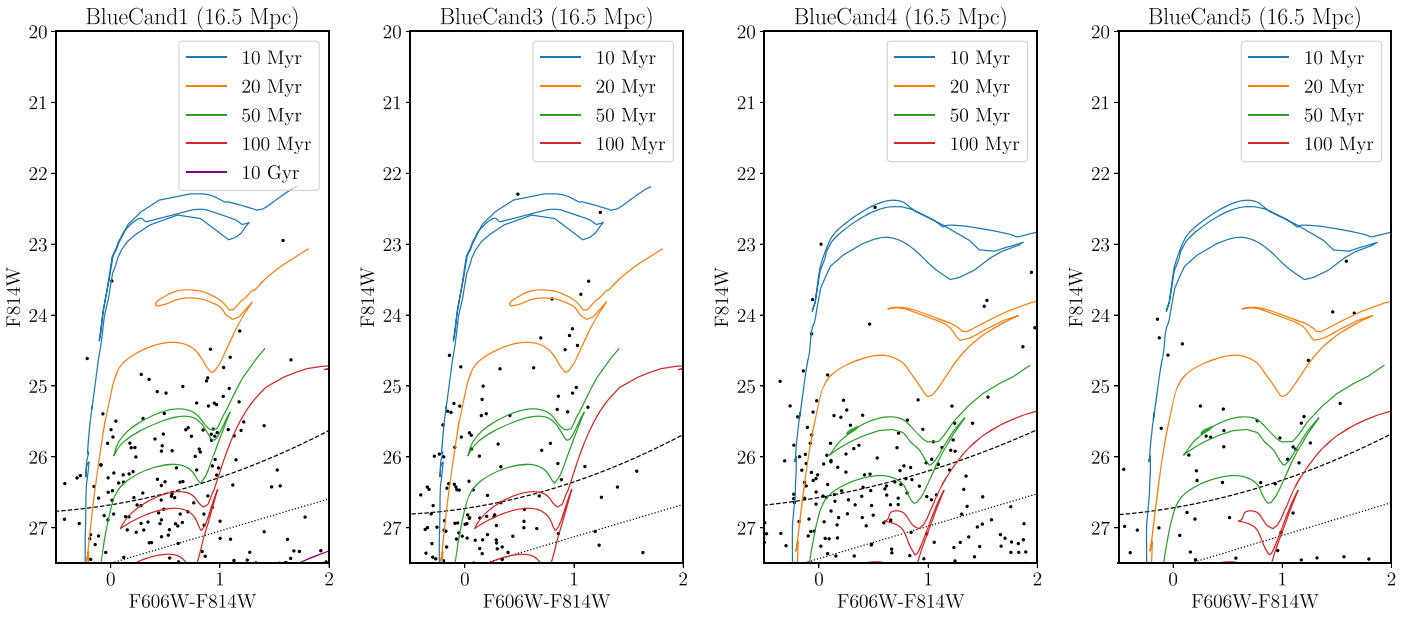

Figure 10. Reproduced CMDs of BCs 1, 3, 4, and 5, with PARSEC isochrones for different stellar population ages overlaid, assuming a distance of 16.5 Mpc to all objects. The isochrones for BC1 and 3 use a metallicity of $[M/H] = -0.35$, which is approximately the value for both objects. For BC4 and 5, the value is $[M/H] = 0.05$. In the latter case, it is possible that the two objects are associated, while the similar metallicities of BC1 and 3 are likely by chance. In the leftmost panel, we also plot an isochrone indicating where an old (10 Gyr) RGB population would reside in these diagrams, below the completeness limit in the lower right corner and barely visible.

Sand et al. (2017) also simulate a mock stellar population and argue that SECCO 1 must be younger than ∼50 Myr based on the luminosity of the RHeB stars. This is roughly consistent with our estimate of 60 Myr in Section 4.6 based on the integrated F814W magnitude and SFR of SECCO 1.

If we compare the CMDs of the BCs to the low-mass, gas-rich dwarf Leo P (McQuinn et al. 2015b), then we see a striking difference. In addition to the young blue stars in Leo P there is also a clear, well-populated RGB at a similar magnitude that is entirely absent from the BCs CMDs. This clear RGB is the result of the old underlying population in Leo P, but for extremely young stellar populations (which BCs appear to be) no RGB population exists. Furthermore, any RGB stars would be significantly less luminous than the young stars that dominate the CMDs of the BCs. However, the proximity of Leo P ($D = 1.6$ Mpc) means that the depth of its CMD is a mismatch for those of BCs, making it an unfair comparison, despite it being one of the most similar objects known in terms of SFR and stellar mass (but notably not metallicity).

A fairer comparison can be made by considering a blue, irregular dwarf at the distance of Virgo, in this case VCC 1816 (KDG 177, $M_V = -15.2$), which has similar depth HST observations as the BCs. The CMD of this galaxy (Figure 4 of Karachentsev et al. 2014) shows both a blue population (at F606W-F814W∼0) and a red population (at F606W-F814W∼1), similar to BCs. The former is likely made up of blue helium-burning stars and young MS stars, as in the BCs, while the latter is likely made up of a combination of asymptotic giant branch and RHeB stars. The number of stars in the CMD increases toward fainter F814W magnitudes (near F606W-F814W∼1) probably indicating the presence of a well-populated RGB near the completeness limit, which is lacking in the BC CMDs. A similar lack of evidence for any RGB was noted for SECCO 1 by Sand et al. (2017) and Bellazzini et al. (2018), but in comparison to a red dwarf spheroidal in Virgo, rather than a star-forming dwarf more in line with the appearance of BCs.

At the distance of the Virgo cluster, the tip of the red giant branch (TRGB) is expected to be at F814W ∼ 27 mag (e.g., Jiang et al. 2019), which would be borderline detectable with our HST observations. However, at high metallicities the TRGB becomes less defined and RGB stars become redder, both of which would impede the detectability of an RGB in our observations (Figure 10, leftmost panel). Thus, it is not possible to conclusively rule out there being an RGB based on the CMDs of BCs. Despite this, we still view the existence of an underlying old population as extremely unlikely in these objects. They are extremely blue, to the point where stellar population models struggle to reproduce their colors, even when assuming very young ages (Section 4.6). In addition, BCs were specifically selected (Section 2) to be lacking any visible diffuse red component in the deep NGVS images. Together these points make it highly unlikely that there could be any significant underlying old population of stars, even though the CMDs themselves are insufficiently deep to reach any potential RGB.

Overall the CMDs of the BCs can be characterized as having a population of stars made up exclusively of young blue main-sequence and (blue and red) helium-burning stars, with no evidence of an RGB. The luminosities of the RHeB stars suggest that the youngest BCs (BC3 & SECCO 1) are around 50 Myr old. Finally, the remarkably high metallicities measured with MUSE (Section 4.2) appear to be consistent with the color difference between the reddest and bluest helium-burning branch stars in the CMDs.

4.5. Star Formation Rates

SFRs (Table 6) were estimated for each candidate by measuring the NUV and FUV fluxes within the same apertures used to produce their CMDs (Section 4.4), as described in

Section 3.3. An additional uncertainty of 15% was added to the error budget as this is the stated accuracy of the conversion in Iglesias-Páramo et al. (2006).

The SFRs of all BCs fall in the range $-3.5 < \log\mathrm{SFR}/\mathrm{M}_\odot\,\mathrm{yr}^{-1} < -3$ and are generally quite consistent between NUV and FUV (where both images are available), likely indicating that their SFRs have not varied strongly over the past ∼100 Myr (or that they are younger than this). Although matching NUV and FUV SFR estimates could be the result of a bursty SF history over the past ∼100 Myr, with an average rate that equals that of the past ∼10 Myr, it seems highly unlikely that this could be the case for all BCs, and a constant SFR is a more natural explanation for this finding. The UV-based SFRs are also roughly consistent with the SFRs estimated from the integrated Hα fluxes (Paper I), with the slight exception of BC1 (for which the SFR may be beginning to decline), again supporting the assertion that the SFRs appear to have been relatively constant in the recent past. We note that had we adopted a different conversion scheme for our UV-based SFR estimates (e.g., McQuinn et al. 2015a), our $\mathrm{SFR}_{\mathrm{FUV}}$ values could be up to 0.6 dex higher. However, given the general consistency between the Hα and UV-based SFR estimates, the conversion scheme we originally selected appears appropriate for these objects.

This range of SFRs is similar to the faintest dwarf irregular galaxies in the Local Volume (Lee et al. 2009). However, the extremely low stellar masses of BCs (Section 4.6) make it difficult to directly compare to equivalent star-forming dwarf galaxies, as almost none are known at these masses. For example, even Leo P (Giovanelli et al. 2013) has almost an order of magnitude higher stellar mass than most BCs, but its SFR is around an order of magnitude lower ($\log\mathrm{SFR}/\mathrm{M}_\odot\,\mathrm{yr}^{-1} = -4.4$; McQuinn et al. 2015b). Leo T (Irwin et al. 2007) is of comparable stellar mass to BCs ($M_* = 1.4 \times 10^5\ M_\odot$; Weisz et al. 2014) but is apparently no longer forming stars or is between episodes (Kennicutt et al. 2008). If we put the SFRs of BCs in terms of their specific SFRs (sSFR), then they fall in the range $-8.2 < \log(\mathrm{SFR}/M_*)/\mathrm{yr}^{-1} < -7.7$, which would place them significantly higher than average, but within the scatter, of sSFR for low-mass, gas-rich, field galaxies (Huang et al. 2012; James et al. 2015).

4.6. Stellar Masses

The integrated F606W and F814W magnitudes of the BCs were measured from the co-added images in each filter. The same apertures indicated in Figures 2, 4, 5, and 6 were used to measure the total magnitude of each source after masking the few clear background galaxies contained within these apertures. Galactic extinction corrections were made using the dust maps of Schlegel et al. (1998) and the reddening R_ν values of Schlafly & Finkbeiner (2011). The final magnitudes are listed in Table 5. The uncertainties were estimated by placing 10 apertures across the full ACS FoV (avoiding bright stars and background galaxies) and using the standard deviation of the counts to approximate the uncertainty in the counts of each BC.

In young stellar populations, the emitted light is dominated by the youngest stars, but the mass is generally dominated by the oldest, most numerous stars. As BCs are apparently such young objects, the correct mass-to-light ratio to use is highly uncertain and would depend strongly on the assumed age of each object. Thus, widely used mass-to-light ratio prescriptions (e.g., Zibetti et al. 2009; Taylor et al. 2011) cannot be used with confidence for such a young, irregular, low-mass, and metal-rich stellar population. We therefore adopt an unconventional strategy for estimating the stellar masses of the BCs. If the current SFRs are assumed to be reasonable representations of the SFRs over the (short) lifetimes of the BCs, then the total stellar mass is simply the age of each object times its SFR. In order to estimate the age, we build up the integrated F814W magnitude of a stellar population forming stars at a constant rate (in 10 Myr steps), based on the PARSEC (Bressan et al. 2012) population models. When the artificial F814W magnitude equals the measured magnitude, we obtain an age estimate for the BC in question (to the nearest 10 Myr).

Table 5
Magnitudes and Stellar Mass Estimates

Object	F814W	F606W-F814W	$M_*/\mathrm{M}_\odot$
BC1	20.29 ± 0.38	0.08 ± 0.41	$\sim 5 \times 10^4$
BC3	20.23 ± 0.15	-0.23 ± 0.17	$\sim 5 \times 10^4$
BC4	19.86 ± 0.26	-0.26 ± 0.29	$\sim 1 \times 10^5$
BC5	20.56 ± 0.10	0.06 ± 0.12	$\sim 5 \times 10^4$
SECCO1	20.39 ± 0.41	-0.23 ± 0.46	$\sim 4 \times 10^4$

Note. Columns: (1) object name; (2) F814W magnitude (extinction corrected); (3) F606W-F814W color (extinction corrected); (4) stellar mass estimate (Section 4.4).

To estimate the ages, and subsequently the stellar masses (age × SFR), we used the NUV SFR measurements (Table 6) for each object, as these are available for all objects and reflect a slightly longer SF timescale. For BC1, BC3, and SECCO1 a metallicity of $[M/H] = -0.35$ was used, and $[M/H] = 0.05$ for BC4 and BC5. These values approximately correspond to their observed O/H values (Table 3). The age estimates[25] for BCs 1, 3, 4, 5, and SECCO 1 are 90, 50, 110, 160, and 60 Myr, and the resulting stellar mass estimates are shown in Table 5.

A significant caveat to this approach is that the PARSEC models are incapable of correctly reproducing the colors of the BCs (as noted by Sand et al. 2017). Although this issue is not fully addressed in this work, we chose to rely on the F814W magnitudes as the discrepancy is assumed to be most severe for the youngest, bluest stars. Hence the redder band is expected to be somewhat less impacted. We also note that there are encouraging trends in the values that we obtained, that at least indicate internal consistency. For example, BC3 and SECCO 1 are the only BCs detected in H I and we estimate these are by far the youngest objects—a finding that the CMDs of the BCs would also seem to support. The estimated ages of BC4 and BC5 are also the oldest, and it seems plausible (Section B.2) that the two formed from the same origin. In addition, Junais et al. (2021) independently estimated the stellar mass of BC3 by fitting the spectral energy distribution (from photometry in *ugriz*, Hα, NUV, and FUV) of each clump with a single stellar population, via a grid search over metallicity and population age, and found a near identical value ($\sim 5 \times 10^4\ M_\odot$).

[25] We note that these age estimates should be treated with caution. Ideally the full SF histories of the BCs would be calculated, but the currently existing data are inadequate to do this. These ages represent an approximation to the age of the oldest stellar population in each BC, based on the assumption of a roughly constant SFR.

Table 6
UV Fluxes and SFR Estimates

Object		SNR_{NUV}	NUV flux	$\log \frac{SFR_{NUV}}{M_\odot\,yr^{-1}}$	SNR_{FUV}	FUV flux	$\log \frac{SFR_{FUV}}{M_\odot\,yr^{-1}}$	$\log \frac{SFR_{H\alpha}}{M_\odot\,yr^{-1}}$	$\log \frac{M_{HI}\,/\,SFR}{yr}$
BC1		10.1	9.10 ± 0.90	-3.25 ± 0.08	13.7	1.98 ± 0.14	-3.42 ± 0.07	-3.9	< 9.5
BC3			17.4 ± 0.7	-3.03 ± 0.07		4.02 ± 0.09	-3.18 ± 0.07	-3.1	10.3
	a	23.8	14.1 ± 0.6	-3.13 ± 0.07	43.9	3.36 ± 0.08	-3.26 ± 0.07		
	b	9.3	2.78 ± 0.30	-3.83 ± 0.08	13.6	0.57 ± 0.04	-4.03 ± 0.07		
	c	4.6	0.57 ± 0.12	-4.52 ± 0.11	5.6	0.10 ± 0.02	-4.77 ± 0.10		
BC4			13.1 ± 0.7	-3.10 ± 0.07				-3.2	< 9.6
	a	16.5	4.07 ± 0.25	-3.60 ± 0.07					
	b	4.7	1.04 ± 0.22	-4.20 ± 0.11					
	c	11.8	2.37 ± 0.20	-3.84 ± 0.08					
	d	6.1	1.49 ± 0.24	-4.04 ± 0.10					
	e	7.4	3.56 ± 0.48	-3.66 ± 0.09					
	f	4.1	0.55 ± 0.13	-4.47 ± 0.13					
BC5			6.13 ± 0.31	-3.48 ± 0.07		1.20 ± 0.05	-3.69 ± 0.07	-3.8	< 10.0
	a	20.1	5.57 ± 0.28	-3.52 ± 0.07	27.4	1.13 ± 0.04	-3.72 ± 0.07		
	b	2.8	0.38 ± 0.14	-4.68 ± 0.16	2.8	0.06 ± 0.02	-4.96 ± 0.16		
	c	3.7	0.18 ± 0.05	-4.99 ± 0.12	1.3	0.01 ± 0.01	-5.67 ± 0.33		
SECCO1			10.4 ± 0.8	-3.14 ± 0.07				-3.2[a]	10.3
	MB	11.1	6.72 ± 0.06	-3.33 ± 0.08					
	SB	7.6	3.63 ± 0.48	-3.60 ± 0.09					

Note. Columns: (1) object name and subcomponent (where relevant); (2) SNR of NUV emission (see Section 4.5 for details); (3) NUV flux in units of 10^{-17} erg s^{-1} cm^{-2} $\AA^{-1}$; (4) NUV-based SFR estimate; (5) SNR of FUV emission; (6) FUV flux in units of 10^{-16} erg s^{-1} cm^{-2} $\AA^{-1}$; (7) FUV-based SFR estimate; (8) Hα SFR estimates from the integrated Hα flux of each object in MUSE (Paper I) following the conversion of Kennicutt (1998); (9) gas consumption timescale using the larger of the NUV and FUV SFR estimates (we note that this quantity is distance independent). For uniformity, all objects are assumed to be at 16.5 Mpc.
[a] Hα-based SFR estimate from Beccari et al. (2017a, 2017b).

5. Points of Origin

The observations presented above reveal the surprising result that, although all the BCs are actively forming stars, only BC3 and SECCO 1 have a detectable quantity of H I. However, the typical values of the SFR estimates are of the order of 10^{-3} $M_\odot$ yr^{-1} (Table 6), which means that even below our H I detection limits (Section 4.3), these objects could still have gas consumption timescales in excess of 1 Gyr (although such long timescales are not uncommon for low-mass galaxies). In addition, the high metallicities of BCs (Table 3) clearly point to them all having formed from pre-enriched gas that originated in a larger galaxy, as has been shown explicitly to be the case for BC3 (Jones et al. 2022), where the gas trail can still be traced back to its parent galaxy.

Figure 11 compares the metallicities of BCs to other objects of comparable luminosity. As expected, Tidal Dwarf Galaxies (TDGs) are similar to BCs, being of equivalent metallicity, but typically somewhat higher luminosities. This is a point to which we will return in the following section (Section 6), but BCs are likely too low mass to be TDGs. On the opposite end of the metallicity spectrum, we compare BCs to a small selection of extremely metal-poor galaxies (XMPs). These objects can appear superficially similar to BCs. Both are usually extremely blue, have clumpy morphologies, and the faintest XMPs are the same luminosity as BCs. However, their metallicities could scarcely be more different, and the two populations are clearly distinct in origin.

If we take the metallicities of the BCs and use them to infer a stellar mass from the mass–metallicity relation (MZR), then this should provide a reasonable estimate of the type of galaxies from which they formed. Using the MZR of Andrews & Martini (2013), the metallicities of the BCs imply that their parent objects could have stellar masses anywhere in the range $8.3 \lesssim \log M_*/M_\odot \lesssim 10.1$ (we note that because the MZR is an asymptotic relation, the lower bound of this range is much better constrained than the upper bound). This covers a broad range from dwarf galaxies almost to Milky Way–like galaxies ($\log M_{*,MW}/M_\odot = 10.8$; Licquia & Newman 2015), but all are massive enough that, unless they have particularly low-surface brightness (LSB), they should be mostly included in existing catalogs of Virgo cluster galaxies. Furthermore, it is also reasonable to assume that the parent objects are gas-bearing (or were in the recent past), as they must have been able to supply

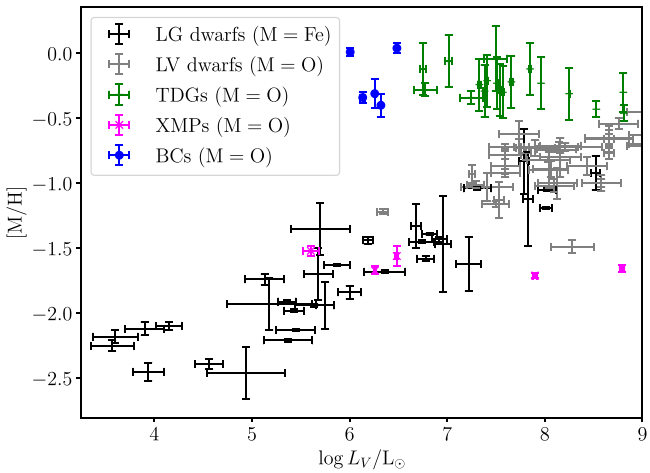

Figure 11. *V*-band luminosity vs. metallicity (relative to solar) for BCs, Local Group dwarfs (Kirby et al. 2013), Local Volume dwarfs (Berg et al. 2012), TDGs (Duc & Mirabel 1998; Weilbacher et al. 2003; Duc et al. 2007; Croxall et al. 2009; Lee-Waddell et al. 2018), and extremely metal-poor galaxies (Skillman et al. 2013; McQuinn et al. 2015b; Hirschauer et al. 2016; Hsyu et al. 2017; Izotov et al. 2019; McQuinn et al. 2020). Metallicity is measured either from Fe/H or O/H as indicated in the legend. Both BCs and TDGs sit well above the luminosity–metallicity relation for dwarf galaxies of equivalent luminosities.

the gas that formed the young stellar populations of the BCs. The quoted range is for the average metallicity and does not account for metallicity variations within the parent galaxies, which could potentially expand the range if the material that formed a BC originated from a region that strongly deviated from the average metallicity.

5.1. Search for Points of Origin

We performed a detailed search considering all known Virgo members in the vicinity (and at a similar velocity to) each BC, paying particular attention to gas-bearing galaxies detected in ALFALFA (Haynes et al. 2018). Even though most BCs are undetected in H I, they appear to have formed from stripped gas and must have contained gas in the recent past as they have all formed stars recently. Thus, nearby, gas-rich galaxies are good candidate progenitor systems. The galaxies neighboring each BC are shown in Figures 12 and 13. Here we present the conclusions of our search, but the full details can be found in Appendix B.

Within the entire 4 deg^2 region shown around BC1 in Figure 12 (top left), there is only one galaxy that contains H I gas and is sufficiently massive to have formed a BC, NGC 4579. This galaxy is approximately 140 kpc (30′) to the SW of BC1 and separated from it in velocity by $\sim$400 km s^{-1}. Thus, BC1 would have needed a large ejection velocity (>500 km s^{-1} in total) for NGC 4579 to be its parent object. Furthermore, other than a slightly H I-deficient disk,[26] NGC 4579 shows little sign of recent disturbance in either its H I or CO morphology and kinematics (Chung et al. 2009; Brown et al. 2021). Finally, NGC 4579 appears to be too metal-rich ($12 + \log(O/H) = 8.87 \pm 0.05$; De Vis et al. 2019) to match the metallicity of BC1 ($\langle 12 + \log(O/H) \rangle = 8.35 \pm 0.15$). Thus, NGC 4579 does not seem to be a viable candidate point of origin for BC1, and the genuine point of origin must presumably be beyond the region shown in Figure 12 (> 280 kpc away), but we are unable to identify any strong candidates this far away.

BC3 (also called AGC 226178) was discussed in detail by Jones et al. (2022). This is an extremely complicated field with multiple foreground systems projected on it. BC3's nearest apparent neighbor is NGVS 3543 (also called AGC 229166), which Junais et al. (2021) argued was an LSB galaxy at the same distance as BC3. However, based on the CMDs produced from HST imaging, Jones et al. (2022) demonstrated that NGVS 3543 is a foreground object at $\sim$10 Mpc, while BC3 is consistent with being in Virgo at 16.5 Mpc. H I observations with the VLA (Cannon et al. 2015) and Arecibo (Giovanelli et al. 2005; Haynes et al. 2011; Minchin et al. 2019) indicate a possible bridge between BC3 and a pair of galaxies, VCC 2034 and 2037. However, the closer (in projection) of these, VCC 2037, is actually another foreground object at approximately 10 Mpc (Karachentsev et al. 2014). Thus, VCC 2034 ($cz_{\odot} = 1507$ km s^{-1}), $\sim$70 kpc to the SW, is the likely source of BC3's H I gas. However, Jones et al. (2022) were unable to determine whether ram pressure or tidal stripping was responsible for removing the gas from VCC 2034.

BC4 and BC5 likely formed from the same parent object as they are only separated by 45′ on the sky, are at almost the same velocity (Table 3), have nearly identical metallicity measurements (Table 3), and have similar age estimates (Section 4.6). NGC 4419 is in fairly close proximity to both BCs and based on its estimated stellar mass and metallicity, it is likely a close match for the metallicity of these BCs. In addition, there is strong evidence in both H I (Chung et al. 2009) and CO (Brown et al. 2021) that this galaxy is being ram pressure stripped. However, as ram pressure tails only extend in one general direction (in the wake of a galaxy's motion through the ICM) and BC4 is to the south of NGC 4419 and BC5 is to the north, it is extremely unlikely that this is the point of origin of these BCs. The extension of the molecular gas distribution of NGC 4419 is roughly toward the south (Brown et al. 2021), in the direction of BC4, but away from BC5. If NGC 4419 were simultaneously undergoing ram pressure and tidal stripping then it could plausibly have formed both BCs, but there is no evidence of this in the optical, H I, or CO images.

There are a few other gas-bearing galaxies within 1 deg of either BC4 or BC5, but these were all discounted due to a mismatch in properties or because of evidence showing ram pressure stripping in the wrong direction. Upon searching further afield, we immediately identified UGC 7695 (VCC 1450, IC 3476) as a strong candidate. This galaxy is a well-studied example of ram pressure stripping in action (Boselli et al. 2021) and has a prominent bow-shaped wake extending in the approximate direction of BC4 and BC5. Existing measurements of the metallicity of UGC 7695 (Hughes et al. 2013; Boselli et al. 2021) also approximately match those of BC4 and BC5, making this a promising candidate for their point of origin. As the separation between the BCs and UGC 7695 is approximately 450 kpc in projection they would presumably require a very large (perhaps over 1000 km s^{-1}) ejection velocity, depending on when the stripping episode began.

Finally, we consider SECCO 1. Figure 13 shows the neighbors of SECCO 1 within a 4 deg^2 field and $\pm$500 km s^{-1} and demonstrates the extraordinary isolation of this system given that it is within the virial radius of a cluster. The potential points of origin for SECCO 1 have already been discussed extensively by previous works (Adams et al. 2015; Sand et al. 2017; Bellazzini et al. 2018), and we will only review these briefly here.

If formed by a stripping event then the most likely point of origin is either the M 86 subgroup of Virgo, about 350 kpc to the SE, which exhibits an enormous complex of stripped gas visible in X-rays and Hα (Sand et al. 2017, and references therein), or the group of dwarf galaxies $\sim$200 kpc to the NW (Bellazzini et al. 2018). The proximity of VCC 322, 334, and 319 (compared to the M 86 subgroup) might favor this possibility. However, as we have discussed above, in some cases the separation between parent and BC may be quite large. What is a stronger argument is that the metallicities of VCC 322 and 334 are a close match to that of SECCO 1 (Bellazzini et al. 2018). VCC 322 also has a stellar tail that extends in the general direction of SECCO 1. Although these galaxies are less massive than some of the others considered, we note that the apparent parent object of BC3 is also a dwarf galaxy and only a few times more massive than BC3 itself.

However, the complex of stripped gas (e.g., Boselli et al. 2018) in the M 86 subgroup is also a good candidate point of origin, for example, if NGC 4438 (VCC 1043; beyond the FoV shown in Figure 13) fell toward this subgroup via the location of SECCO 1. In this case, a combination of ram pressure and tidal forces could

[26] Chung et al. (2009) define the H I-deficiency of a galaxy's disk as the logarithmic decrement between the observed and expected mean H I surface density within the optical disk, where for the latter they use the average value for isolated galaxies from Haynes & Giovanelli (1984).

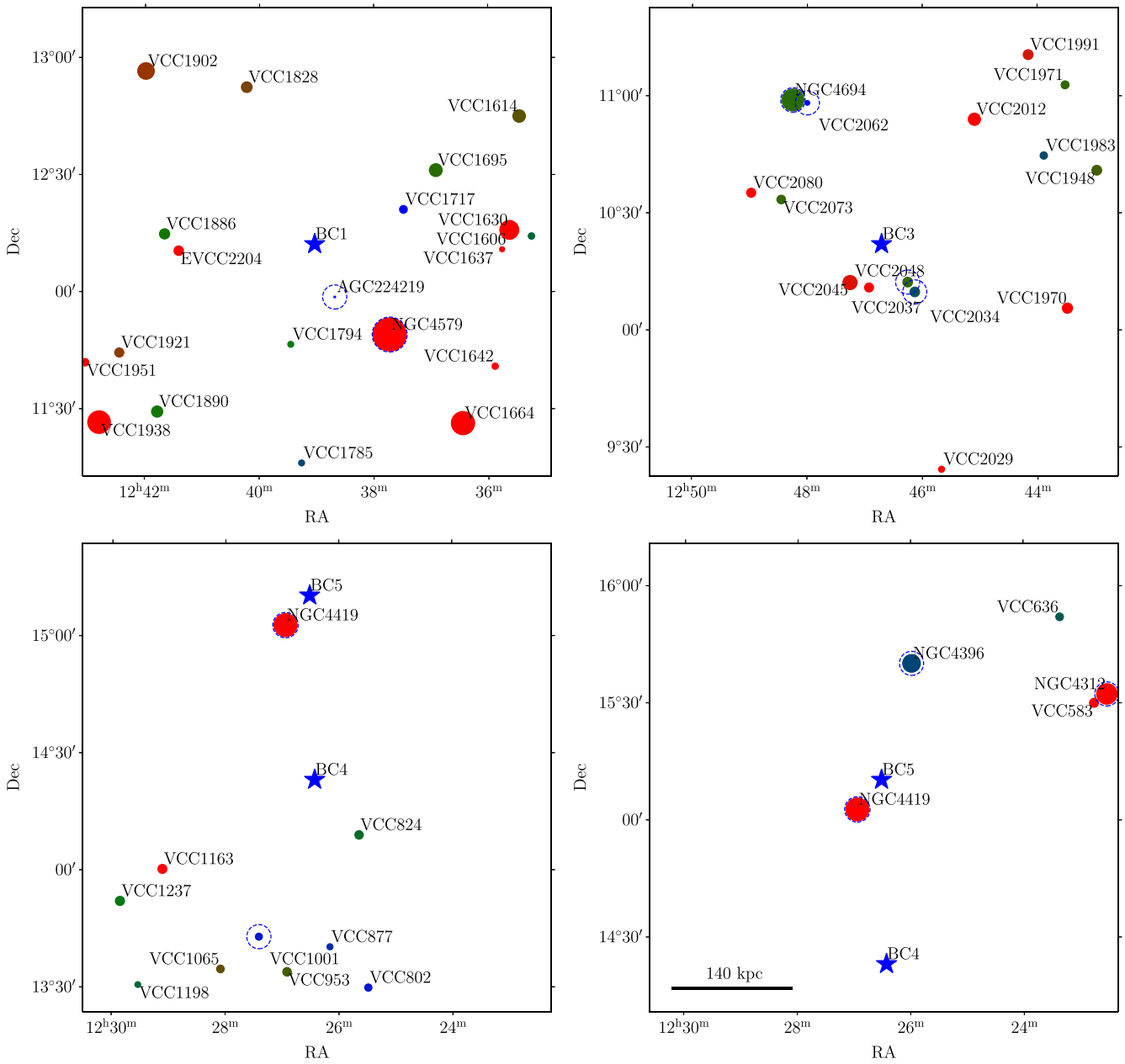

Figure 12. All VCC, EVCC, and ALFALFA neighbors of BC1, 3, 4, and 5 (top left to bottom right) in a 4 sq deg region centered on the BC (blue star in each panel) and within ± 500 km s^{-1} of their Hα velocity (Table 3). The area of each circular marker corresponds to the apparent magnitude (in the g band) of the galaxy it represents. The color of the markers corresponds to the galaxy's $g-i$ color, with the narrow transition from blue to red occurring at $g-i=0.9$ (green). Objects circled with a dashed blue line were detected in ALFALFA and thus contain significant quantities of H I (note that BC3 itself was detected in ALFALFA, but is not circled here). At the distance of Virgo 30′ corresponds to ∼140 kpc. The scale bar in the bottom-right panel applies to all panels.

be responsible for SECCO 1 and the complex of stripped gas. We also noted the blue dwarf irregular IC 3355 near NGC 4438 (in the approximate direction of SECCO 1). However, the lower metallicity of this object ($12+\log(\mathrm{O/H}) \approx 8.0$; De Vis et al. 2019) suggests that it did not form from stripped gas.

5.2. Other Origin Scenarios

In the above discussion we considered that BCs were likely formed from a gas-bearing galaxy sufficiently massive to be included in existing catalogs of Virgo cluster galaxies. However, there are a few other scenarios that we briefly consider here.

Junais et al. (2021) suggested that BC3 might have formed from gas stripped from an LSB galaxy. Although this scenario is ruled out for BC3 itself (as the LSB galaxy in question is actually a foreground object; Jones et al. 2022) it is possible that LSB galaxies have been missed in our search above, as they are frequently absent from established catalogs of cluster members. In general this mechanism would imply that the LSB galaxy being stripped would be relatively close by to the BC, as it would presumably have a smaller gas reservoir (that would evaporate more rapidly when stripped) than a larger galaxy. Therefore, even though LSB galaxies can be challenging to detect, it seems unlikely that a close neighbor would have been overlooked in multiple cases, and we do not consider this a

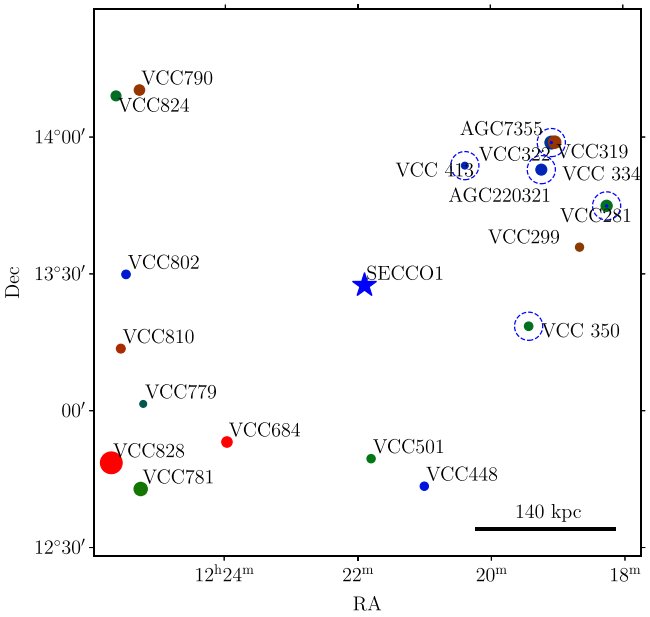

Figure 13. As for Figure 12 but for SECCO 1.

likely formation pathway, but note that it is difficult to entirely exclude.

An additional scenario that we considered is the possibility that the BCs could be dark objects that contained neutral gas for an extended period, but formed essentially no stars until very recently (e.g., Kent et al. 2009; Minchin et al. 2019). This scenario is highly unlikely for two main reasons. First, the search for bona fide dark galaxies that cannot be explained as tidal or spurious objects has turned up few convincing results to date (e.g., Taylor et al. 2013; Cannon et al. 2015), calling into question whether this scenario is valid. Second, the high metallicity of the BCs indicates that there have been multiple prior SF episodes that have enriched their gas, thus ruling out that they could be primordial dark objects (e.g., Corbelli et al. 2021).

6. Formation Mechanism

As shown in Figure 11, the universally high metallicities of BCs (in relation to their luminosities or stellar masses) mean that the only plausible mechanism for their formation is that they formed from material stripped from a larger galaxy. Their metallicities are a full order of magnitude higher than those of galaxies of the same *V*-band luminosity, and owing to their extremely young stellar populations, this discrepancy would be even larger if the samples were compared in terms of their stellar masses. Figure 11 also indicates that BCs are of slightly lower luminosity than TDGs but of similar metallicity. Their stellar and H I masses indicate that BCs are considerably less massive than long-lived TDGs.

Despite the strong evidence that BCs formed from stripped material, it is unclear whether they formed through tidal or ram pressure stripping. As is the case for BC3, even when the H I connection to the parent galaxy is still detectable (Jones et al. 2022), it may not be possible to distinguish between ram pressure or tidal forces as the dominant mechanism stripping the gas. Indeed it is possible that both are valid mechanisms.

Regardless of the mechanism by which gas is stripped to form BCs, the parent objects must be new cluster members. Oman & Hudson (2016) and Oman et al. (2021) simulated the stripping and quenching of galaxies falling into clusters and found that essentially all new members are stripped of their gas and quenched during their first orbit, usually around pericenter passage (see also Cortese et al. 2021; Boselli et al. 2022, for reviews). Thus to have sufficient gas to form a BC, the parent galaxy must likely be on its first infall into the cluster. Although we only have a sample of five objects, this would also appear to agree with their spatial distribution which is inside the virial radius, where significant stripping is expected, but avoids the cluster center.

In the remainder of this section we discuss the evidence for and against tidal and ram-pressure formation scenarios, compare BCs to other classes of objects known to form from stripped gas, and give an overview of related simulation results.

6.1. Comparison to TDGs and the Need for Ram Pressure Stripping

The typical masses of long-lived TDGs are expected to be over $10^8\,M_\odot$ (Bournaud & Duc 2006), as below this mass they generally cannot resist the tidal field of their parent galaxies for long enough to escape as bound objects. This threshold mass is considerably larger than any of the BCs, disfavoring a tidal formation pathway, as the most massive BCs (BC3 and SECCO 1) are a few times $10^7\,M_\odot$. However, we note that if a lower-mass TDG were to be ejected at particularly high speed it may be able to survive, as it would more rapidly escape the tidal field of its parent galaxy. We also note that the simulations of Bournaud & Duc (2006) assume that the parent object of TDGs are loosely MW-like; however, VCC 2034 (the apparent parent object of BC3; Jones et al. 2022) has a stellar mass of only $10^{8.2}\,M_\odot$. If BCs are tidal in origin then perhaps they formed from lower-mass progenitors and are correspondingly lower mass than typical long-lived TDGs. However, such a mechanism could presumably only apply to those BCs (BC1, BC3, and SECCO 1) with slightly lower metallicities that correspond to similarly low-mass progenitors (via the MZR), unless the more metal-rich BCs (BC4 and BC5) formed from recently enriched gas that was stripped before it had sufficient time to mix with the rest of the interstellar medium in the parent galaxy.

TDGs are typically ejected at around the circular velocity of the galaxy they originate from (Bournaud & Duc 2006). For a relatively massive galaxy this might mean an ejection velocity of $\sim$300 km s^{-1}. If this were preferentially aligned along the direction perpendicular to the line of sight, it would still take a TDG $\sim$1 Gyr to traverse 300 kpc in projection. Thus the isolation of BCs, coupled with their very young stellar populations, is difficult to explain via a tidal formation mechanism. In contrast, in the case of ram pressure stripping the velocity of the galaxies relative to the cluster can exceed 1000 km s^{-1}, and galaxies with the largest tails are generally found to be traveling at highest speeds (Jaffé et al. 2018). The fact that BCs have been identified in a cluster also points to ram pressure stripping as the most likely formation pathway. All gas-rich galaxies falling with sufficient velocity into a cluster are expected to undergo some degree of ram pressure stripping, and while tidal interactions are certainly commonplace in clusters, these most frequently take the form of brief, high-speed encounters (e.g., "galaxy harassment"), which are less likely to strip large quantities of gas (e.g., Smith et al. 2010)

than the strong, drawn-out interactions in galaxy groups (where TDGs are typically found).

However, although the relative velocity between an infalling galaxy and the ICM can easily exceed 1000 km s^{-1}, this does not necessarily translate into an equivalent velocity for the stripped gas, as once stripped it does not immediately become stationary relative to the ICM. The ram pressure stripping simulations of Kapferer et al. (2009) consider gas-rich galaxies falling at 1000 km s^{-1} relative to an ICM of varying densities (from 1×10^{-28} to 5×10^{-27} g cm^{-3}). They show that after 500 Myr of stripping the length of the plume of stripped gas in the wake of the parent galaxy is strongly dependent on the density of the surrounding ICM (e.g., their Figure 20). In this case the most distant gas clouds (for $\rho_{\rm ICM}\geqslant1\times10^{-27}$ g cm^{-3}) are ∼400 kpc from their parent galaxy, indicating that their average relative velocity over the past 500 Myr has been ∼800 km s^{-1}. This is somewhat slower than the velocity of the parent galaxy relative to the ICM (and would be considerably slower still for lower ICM densities) but is still several times greater than the relative velocities typically expected for TDGs. For comparison, the electron number density of the ICM in Virgo (Nulsen & Bohringer 1995) exceeds 10^{-2} cm^{-3} ($\sim2\times10^{-26}$ g cm^{-3}) near M 87 and at a distance of 230 kpc has decreased to 6×10^{-4} cm^{-3} ($\sim1\times10^{-27}$ g cm^{-3}). Thus ram pressure stripping (in Virgo) provides a more viable mechanism for rapidly achieving large separations between stripped material and its parent object. This is especially true within a few hundred kiloparsecs of the cluster center but could be true almost anywhere within the cluster should an infalling galaxy collide with a dense pocket in the ICM (which are known to exist in other clusters; e.g., Morandi & Cui 2014; Eckert et al. 2015).

The most similar known objects to BCs are "fireballs" (e.g., Cortese et al. 2007; Yoshida et al. 2008; Hester et al. 2010), clumps of SF seen in the wake of galaxies being actively ram pressure stripped. Indeed, as discussed by Bellazzini et al. (2018), many of the properties of BCs match well with those of fireballs (e.g., Fumagalli et al. 2011), including their metallicities (e.g., fireballs in the wake of IC 3418 have $8.22<12+\log({\rm O/H})<8.38$; Kenney et al. 2014). Other related objects include SF clumps in filamentary structures in the vicinity of NGC 1275 in the Perseus cluster (Conselice et al. 2001; Canning et al. 2014) and in stripped material in Stephan's Quintet (Mendes de Oliveira et al. 2004).

However, BCs are distinct from fireballs and similar objects, in that they are remarkably isolated (e.g., Figures 12 & 13). Fireballs are found within a few 10 s of kpc of their parent galaxy, where there can be little doubt over their point of origin, and where they may still eventually fall back onto their parent galaxy (e.g., Vollmer et al. 2001; Tonnesen & Bryan 2012a). To form BCs requires a mechanism which can carry neutral gas several 100 s of kpc from a galaxy within the hostile environment of a cluster.

6.2. Properties of Ram Pressure Stripped Gas Clumps in Simulations

Lee et al. (2022) argue that many of the molecular gas clouds seen in the tail of ram-pressure-stripped galaxies (e.g., Moretti et al. 2018; Jáchym et al. 2019) could form in situ, by rapid cooling of warm ionized gas (Tonnesen & Bryan 2012b; Moretti et al. 2020, also suggest a similar mechanism). The metal-rich gas and absence of young stars in close proximity (unlike within the disks of most gas-rich galaxies) make conditions favorable for radiative cooling. Furthermore, Müller et al. (2021) argue that magnetic sheathing could help to protect ram-pressure-stripped gas from evaporation in a cluster environment.

In the radiative hydrodynamical simulations of Lee et al. (2022) SF clumps are seen out to ∼100 kpc from the parent galaxy. In their models this SF in the distant tail occurs ∼200 Myr after the initial onset of ram pressure stripping, suggesting that the very young ages (50–150 Myr) of the stellar populations of BCs may underestimate how long ago their progenitor gas was stripped (although large velocities >500 km s^{-1} would likely still be required to explain their isolation). Finally they note that although bright Hα clumps will only track SF activity, more diffuse Hα emission (fainter than 6×10^{38} erg s^{-1} kpc^{-2}) is expected throughout the ram pressure tail due to recombinations in the warm ionized gas. Therefore, Hα observations significantly more sensitive than this threshold might be capable of robustly identifying the points of origin of BCs. The nominal 1σ surface brightness sensitivity of the Virgo Environmental Survey Tracing Ionised Gas Emission (VESTIGE) survey is 2×10^{-18} ergs s^{-1} cm^{-2} arcsec^{-2} (Boselli et al. 2018), which for a distance of 16.5 Mpc equates to 3.4×10^{36} erg s^{-1} kpc^{-2}. Thus, such features, should they exist, would be detectable in VESTIGE.

The hydrodynamic simulations of Kapferer et al. (2009) also produce numerous gas clumps in the wakes of ram-pressure-stripped galaxies, but out to much greater distances (∼400 kpc). They find that SF is only induced in these clumps if the wind speed exceeds 500 km s^{-1} and that it is enhanced by yet stronger ram pressure (but note that Tonnesen & Bryan 2012b, find the opposite trend). Ram pressure therefore appears to be a promising candidate for producing clumps of star-forming gas far from their parent galaxies, but do the physical properties of these systems match with those observed in BCs?

In the case of the above mentioned ram pressure simulations the gas clumps in the wakes of the stripped galaxies are generally presented in terms of gas density rather than masses of distinct clumps. However, in the simulations of Tonnesen & Bryan (2021) the masses of such clumps are found to be on the order of $10^5\,M_\odot$, with the most massive distinct clouds being $\sim10^6\,M_\odot$. This matches quite well with the masses of gas clumps typically found in the immediate wakes of ram-pressure-stripped galaxies (e.g., Poggianti et al. 2019), but is more than an order of magnitude less massive than BC3 and SECCO 1. However, the earlier ram pressure stripping simulations of Kronberger et al. (2008) do form bound objects, analogous to TDGs, with total masses of $\sim10^7\,M_\odot$, but these simulations are now thought to oversimplify fluid instabilities (e.g., Sijacki et al. 2012), calling into question the details of these results.

It terms of metallicity it is generally assumed that, in either the tidal or ram pressure stripping scenario, the BC formed will exhibit the same metallicity as its parent galaxy. However, Tonnesen & Bryan (2021) also find that all their simulated ram-pressure-stripped clouds rapidly mix with the ICM. Thus, they predict that the metallicity of ram-pressure-stripped clouds should decrease with the distance from their parent galaxy. This seems to be directly contradicted by the high metallicities of BCs, given their relative isolation and large separations (e.g., >300 in some cases) from their apparent points of origin. We also note that Calura et al. (2020) find that more massive H I clouds (similar to SECCO 1 and BC3) can survive intact for times on the order of 1 Gyr, while moving rapidly through the

ICM. It may be that the gas clouds from which BCs form are exceptional objects and not typical of the underlying population of gas clouds that are stripped in ram pressure events. For example, these could be some of the most loosely bound gas that is the first to be stripped, or they could be stripped by a denser clump of the ICM. This could explain the lack of similar objects in the simulations of Tonnesen & Bryan (2021).

As a closing remark for this discussion we also note that despite the apparently simple requirement for ram pressure stripping (i.e., sufficient ram pressure to overcome the gravitational attraction of the gas disk) and extensive efforts to simulate this process in increasing detail, there remain systems that are challenging to explain. In particular, the recent discovery of an enormous (apparently) ram-pressure-stripped H I tail in a system outside of a cluster, where no significant intergalatic medium could be detected (Scott et al. 2022), poses difficult questions regarding its origin and could even suggest that some BC-like objects might exist outside of clusters.

6.3. Summary

In summary, BCs appear to be distinct from both TDGs and fireballs, being too low-mass to be the former, too high-mass to be the latter, and too isolated for either. The isolation of some BCs is their property that is the hardest to explain, and would seem to necessitate the large velocities expected in ram pressure stripping events, but not for strong tidal interactions. We therefore favor ram pressure stripping as the most likely formation mechanism of BCs. If ram pressure stripping is confirmed to be the formation pathway then BCs can be thought of as "ram pressure dwarfs", analogous to tidal dwarfs, but unlikely to survive as bound structures on long timescales. Simulations provide a somewhat conflicting picture of how such objects might form via ram pressure stripping; however, this may be because BCs represent atypical objects that, unlike fireballs, are not formed in large numbers during stripping episodes. Regardless of their formation mechanism the properties of BCs appear to be distinct from any other stellar systems of which we are aware.

7. Fate and Production Rate

Based on their morphologies and stellar mass estimates, BCs are unlikely to be gravitationally bound. In the case of BC3 and SECCO 1, their H I content might be sufficient for them to remain bound in the short term (e.g., Calura et al. 2020), but this neutral gas (the majority of their total mass) will eventually be lost to the ICM. It is challenging to accurately assess the stability of BCs due to their irregular morphologies and because their velocity dispersions are not well resolved by the MUSE observations. However, based on the stellar mass estimates in Table 5 and their apparent sizes, we estimate that if they are extremely dynamically cold (e.g., $\sigma_v < 1$ km s^{-1}) then they may be bound, but for $\sigma_v > 2$ km s^{-1} they would certainly be unbound (using Equation (8) of Calura et al. 2020). The stability of BCs is considered further in Paper I; however, the most likely scenario is that each BC as a whole is unbound, but individual component clumps or star clusters may be bound, if sufficiently dynamically cold. Thus, in the long term BCs will likely disperse (either as individual stars or star clusters) into the intracluster light. However, even if BCs were to remain bound, without sustained SF they would quickly become essentially undetectable. Currently they are only identifiable at all (in optical/UV) because of their young, blue stars.

In Jones et al. (2022) we argued that as BCs are only expected to be visible for a short period, they must be continually produced in the cluster. We estimated that an object such as BC3 might be detectable for at most 500 Myr, meaning that for five BCs to be visible today, they must be being produced at a rate on the order of 1 per 100 Myr. However, given that all five of the known BCs appear to have ages of less than 200 Myr, this might be a more reasonable estimate, making the production rate closer to 1 per 50 Myr. We speculate that this might be a common phenomenon with many newly infalling galaxies producing such objects.

With this in mind we also note that, in hindsight, the metallicities of BCs are perhaps not surprising. As mentioned in Section 5, the metallicities of BCs correspond to a stellar mass range $8.3 \lesssim \log M_*/\mathrm{M}_\odot \lesssim 10.1$. However, this wide range likely encompasses most galaxies that could possibly form BCs (suggesting it is a common occurrence). Galaxies significantly less massive than $\log M_*/\mathrm{M}_\odot = 8.3$ would have H I reservoirs scarcely larger than those of SECCO 1 and BC3, and are thus probably too small to form a BC themselves. However, galaxies significantly more massive than $\log M_*/\mathrm{M}_\odot = 10.1$ are increasingly uncommon and increasingly likely to be gas-poor.

8. Future Directions

Although the faintness and peculiar properties of BCs make them challenging objects to study, we suggest a few directions where progress could likely be made.

We experienced significant difficulties in attempting to identify the point of origin of most of the BCs, likely because it has been several hundred Myr as some of them were first stripped from their parent galaxy. However, if ram pressure stripping is the formation pathway of these objects, then it is possible that extremely faint Hα trails still connect the BCs to their parent objects (e.g., Lee et al. 2022). A deep Hα search around the BCs (or others identified in the future), is a promising approach to robustly identifying their parent objects, which in turn will allow for a more detailed study of their formation mechanism. X-ray emission is also frequently found to accompany Hα tails of ram-pressure-stripped galaxies (e.g., Sun et al. 2007, 2021) and may represent another means to characterizing the properties of the stripping events that formed the BCs in cases where the parent object can be identified.

CO observations with the Atacama Large Millimeter/submillimeter Array (ALMA) have successfully made detections of individual clumps of molecular gas in the wakes of ram-pressure-stripped galaxies (e.g., Jáchym et al. 2019) as well as individual giant molecular clouds in TDGs (Querejeta et al. 2021). If BCs still contain significant quantities of molecular gas (as would be expected based on their recent SF), then they should be readily detectable with ALMA, especially as their high metallicity measurements imply a favorable CO-to-H_2 conversion factor in comparison to other low-mass objects (Bolatto et al. 2013).

Lee et al. (2022) find that ram-pressure-stripped gas clouds may travel for over a hundred Myr before SF occurs in them. Although we are limited by a very small sample size, all of the BCs with slightly older stellar populations estimates ($\gtrsim$100 Myr, rather than ~50 Myr) are undetected in H I. The long gas consumption (by SF) timescales in Table 6 indicate that the gas in these systems is not (for the most part) consumed by SF. BCs 1, 4, and 5 must have contained significant cold gas

reservoirs within the past 200 Myr to permit the formation of their observed stellar populations, and they likely still contain some molecular gas as they have all formed new stars in the past 10 Myr, yet today we find no evidence of any H I content. If BCs have traveled through the ICM for significantly longer than the current age of their stellar populations in order to reach their current state of isolation, perhaps this indicates that it is the SF episode itself that triggers the evaporation of the neutral gas. For example, it seems plausible that an object like SECCO 1 is essentially an earlier stage of an object like BC4 and BC5. Both are broken into two main components, but SECCO 1 has yet to lose its gas, and BC4 appears as though it may be disintegrating (Figure 5). If this were the case then SECCO 1 would likely be on the verge of losing its H I gas. This disagrees somewhat with the findings of Calura et al. (2020). However, those authors note that the details of the SF episode, particularly when it began, are quite uncertain, and we suggest that this possibility might warrant further investigation.

Along similar lines, with the HST observations it has only been possible to characterize the stellar populations of BCs from the stars formed in the past ∼50 Myr. While some BCs may genuinely contain no stars that are older than this, others might. To detect or rule out this older stellar population, and therefore to constrain the full SF histories of BCs, is possible with the James Webb Space Telescope observations (JWST). With a moderate investment of observing time (∼10 hr) JWST is capable of detecting stars several magnitudes below the TRGB, should an RGB exist, at the distance of the Virgo cluster. Such observations would not only determine the age of the oldest stellar component of BCs, but (if RGB stars exist in BCs) would also be capable of conclusively demonstrating Virgo membership via TRGB distance measurements.

Finally, we note that if our hypothesis is correct and BCs are commonly produced when new member galaxies fall into a cluster, then they should exist in other clusters as well as Virgo. Unfortunately, due to how faint BCs are, they would be undetectable in any galaxy clusters significantly farther away than Virgo. We therefore suggest that the Fornax cluster could be a suitable location to extend the search and would represent an independent environment where our findings could be cross-checked. The distance modulus for Fornax is only ∼0.5 mag greater than for Virgo; thus the brightest BCs (Table 5) would likely still be detectable and slightly longer HST observations could provide similar quality CMDs.

The ongoing MeerKAT Fornax survey (Serra et al. 2016; Kleiner et al. 2021) aims to map 12 $\deg^2$ of the cluster in H I. These observations will be approximately 5 times deeper than our pointed VLA observations of BCs and will have a factor of ∼3 times better angular resolution. Thus this survey will be ideal for identifying "dark", dense H I clouds analogous to those in Adams et al. (2013) and Cannon et al. (2015) that led to the discovery of BCs. Furthermore, the improved column density sensitivity will exceed that of ALFALFA and will be readily capable of detecting residual H I streams that might still connect young BCs to their parent objects, as is the case for BC3 (Jones et al. 2022). The Fornax cluster is also the target of both the Next Generation Fornax Survey (Muñoz et al. 2015), *ugi* imaging with the Dark Energy Camera on the Blanco telescope, and the Fornax Deep Survey with the Very Large Survey Telescope (Peletier et al. 2020), which is imaging the Fornax cluster in *ugri* at comparable depth to the NGVS in Virgo. Together these surveys will provide the means to identifying BCs both through their young blue stellar populations and, where it exists, their H I gas.

9. Conclusions

We have presented follow-up HST, VLT/MUSE, VLA (and GBT) observations of five candidate young, blue, faint, stellar systems in the direction of the Virgo cluster that are analogous to SECCO 1. With the exception of one spurious object, we find that these are all comparable to SECCO 1 in terms of their extremely low stellar masses, blue stellar populations, and high metallicities, leading us to conclude that they must have formed from gas stripped from more massive galaxies. However, only one is detected in H I, suggesting that the others have likely survived sufficiently long to lose much of their initial gas content. Some of these objects are also surprisingly isolated, residing several hundred kiloparsecs from the nearest potential source of gas, which poses a challenge for robustly identifying their points of origin.

We considered both tidal and ram pressure stripping scenarios as the potential formation mechanism of these stellar systems. Although we cannot confidently exclude either of these mechanisms, and indeed there may not be one single mechanism responsible for all BCs, ram pressure stripping is most consistent with the observed properties. In particular, the isolation of some BCs is difficult to explain with the low velocities ($\leqslant 300\,\mathrm{km\,s^{-1}}$) expected for ejected TDGs but can more naturally be explained by ram pressure stripping proceeding at $>1000\,\mathrm{km\,s^{-1}}$. In addition, BCs are likely too low mass to be long-lived TDGs. However, gas clumps formed in ram pressure stripping simulations are typically much lower mass than BCs (based on the H I masses of BC3 and SECCO 1), and we suggest that these objects may be atypical and form from the first loosely bound gas to be stripped, or as a result of stripping in a clumpy ICM. These massive clumps ($\sim 10^7\,M_\odot$) of stripped gas moving at high speed can likely survive sufficiently long in the ICM to form the stellar populations observed and to become relatively isolated. However, they will ultimately lose their gas content (the majority of their total mass) and likely become unbound.

BCs therefore represent a new class of stellar system that form from large ($\sim 10^7\,M_\odot$) clumps of pre-enriched stripped gas, are (assumed to be) dark matter free, and are capable of surviving sufficiently long in the hostile ICM to become isolated (>100 kpc away) from their parent galaxies.

A further census of this class of object in the Virgo cluster, and potentially the Fornax cluster, will allow for improved constraints on their lifetimes and how frequently they are produced. However, robust identification of their parent objects will remain challenging, owing to their isolation. Deep, wide-field Hα imaging, to identify diffuse emission, is a potential approach for systems where the majority of the neutral gas has already been evaporated.

The authors thank Kyle Artkop for assistance in identifying blue candidates in Virgo. We also thank Toby Brown and coauthors for providing their X-ray mosaic from archival ROSAT observations of the Virgo cluster. This work is based on observations made with the NASA/ESA Hubble Space Telescope, obtained at the Space Telescope Science Institute, which is operated by the Association of Universities for Research in Astronomy, Inc., under NASA contract NAS5-26555. These observations are associated with program #HST-

GO-15183. Support for program #HST-GO-15183 was provided by NASA through a grant from the Space Telescope Science Institute, which is operated by the Association of Universities for Research in Astronomy, Inc., under NASA contract NAS5-26555. It is also based on observations collected at the European Organisation for Astronomical Research in the Southern Hemisphere under ESO program 0101.B-0376A. This work used both previously unpublished and archival data from the Karl G. Jansky Very Large Array. The National Radio Astronomy Observatory is a facility of the National Science Foundation operated under cooperative agreement by Associated Universities, Inc. The data were observed as part of programs 13A-028 (PI: J. Cannon) and 18A-185 (PI: K. Spekkens). The work used images from the Dark Energy Camera Legacy Survey (DECaLS; Proposal ID 2014B-0404; PIs: David Schlegel and Arjun Dey). Full acknowledgment at https://www.legacysurvey.org/acknowledgment/.

D.J.S. acknowledges support from NSF grants AST-1821967 and 1813708. M.B. acknowledges the financial support to this research from the INAF Main Stream grant 1.05.01.86.28 assigned to the program *The Smallest Scale of the Hierarchy (SSH)*. K.S. acknowledges support from the Natural Sciences and Engineering Research Council of Canada (NSERC). B.M.P. is supported by an NSF Astronomy and Astrophysics Postdoctoral Fellowship under award AST-2001663. E.A.K.A. is supported by the WISE research program, which is financed by the Dutch Research Council (NWO). G.B. acknowledges financial support through the grant (AEI/FEDER, UE) AYA2017-89076-P, as well as by the Ministerio de Ciencia, Innovación y Universidades, through the State Budget and by the Consejería de Economía, Industria, Comercio y Conocimiento of the Canary Islands Autonomous Community, through the Regional Budget. J.S. acknowledges support from the Packard Foundation. M.P.H. acknowledges support from NSF/AST-1714828 and grants from the Brinson Foundation. J.M.C., J.F., and J.L.I. are supported by NST/AST-2009894. R.R.M. gratefully acknowledges support by the ANID BASAL project FB210003. Research by D.C. is supported by NSF grant AST-1814208. A.K. acknowledges financial support from the State Agency for Research of the Spanish Ministry of Science, Innovation and Universities through the "Center of Excellence Severo Ochoa" awarded to the Instituto de Astrofísica de Andalucía (SEV-2017-0709) and through the grant POSTDOC_21_00845 financed from the budgetary program 54a Scientific Research and Innovation of the Economic Transformation, Industry, Knowledge and Universities Council of the Regional Government of Andalusia.

Facilities: Blanco, GALEX, GBT, HST (ACS), ROSAT, VLA, VLT:Yepun (MUSE)

*Software:*DOLPHOT (Dolphin 2000), CASA (McMullin et al. 2007), astropy (Astropy Collaboration et al. 2013, 2018), APLpy (Robitaille & Bressert 2012; Robitaille 2019), Photutils (Bradley et al. 2020), reproject (Robitaille et al. 2020), acstools (Lim et al. 2020), DS9 (Joye & Mandel 2003), dustmaps (Green 2018), Astroalign (Beroiz et al. 2020), Sextractor (Bertin & Arnouts 1996), Aladin (Bonnarel et al. 2000; Boch & Fernique 2014)

Appendix A
VLA Spectrum of BC2

Although the HST imaging of BC2 (Figure 3) indicates that it is a background group of galaxies rather than a blue stellar system at the distance of Virgo, we have included an H I spectrum extracted from the VLA data cube for completeness (Figure 14). As with the other BCs the spectrum is extracted with a beam-sized aperture centered on the optical position of BC2. However, unlike the other VLA spectra this spectrum covers a broader range of velocities as BC2 has no known redshift from Hα emission. As expected, no significant H I signal could be identified.

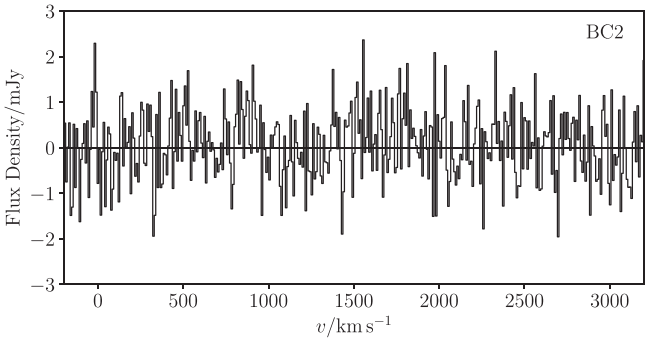

Figure 14. H I spectrum in the directions of BC2 extracted from the VLA H I data cube within an aperture equal in area to the synthesized beam.

Appendix B
Search for Points of Origin

In the following subsections, we search for neighboring galaxies that could have supplied the gas from which the BCs formed. In particular, we consider all ALFALFA (Haynes et al. 2018), Virgo Cluster Catalog (VCC, Binggeli et al. 1985), and Extended Virgo Cluster Catalog (EVCC, Kim et al. 2014) galaxies in the vicinity of each BC, in an attempt to identify the most probable point of origin in each case.

B.1. BC1

As shown in Figure 12 (top left), the nearest galaxy (in projection) with a redshift within 500 km s^{-1} of BC1 ($cz_\odot = 1118$ km s^{-1}), is AGC 224219 (LSBVCC 79), 14.5′ to the SW, which was detected in H I by ALFALFA and AGES (Arecibo Galaxy Environment Survey; Taylor et al. 2013, AGESVC2_30), and marginally detected near the primary beam edge of our VLA observation. After this there is the large spiral NGC 4579 (VCC 1727) further to the SW (30′ in total), which was also detected in H I by ALFALFA.

AGC 224219 ($cz_\odot = 1019$ km s^{-1}) is a very LSB dwarf with a central surface brightness of 24.8 mag arcsec^{-2} in the g band (Davies et al. 2016). Its stellar population is also clearly redder than BC1, which comes as a surprise given that it has at least an order of magnitude more H I. The other progenitor possibility, NGC 4579 ($cz_\odot = 1517$ km s^{-1}) is a much larger, gas-bearing, spiral galaxy. This galaxy was imaged by the VIVA (VLA Imaging of Virgo spirals in Atomic gas, Chung et al. 2009) survey and they concluded that it is slightly H I-deficient and its H I distribution is somewhat truncated (presumably by ram pressure stripping). However, other than this, the H I distribution and kinematics are regular and there is no sign of an ongoing or recent interaction. ALMA (Atacama Large Millimeter Array) observations of its CO molecular gas from VERTICO (Virgo Environment Traced in CO survey; Brown et al. 2021) present a similarly regular morphology. We also note that if BC1 originated from NGC 4579 then it must have had a very large ejection velocity, at least 400 km s^{-1} along the

line of sight. If we also assume BC1 is on the order of 200 Myr in age (e.g., BC3; Jones et al. 2022) then the component perpendicular to the line of sight would need to be on the order of 500 km s^{-1}, giving a total ejection velocity of ∼650 km s^{-1}, a large but not impossible value.

Perhaps both BC1 and AGC 224219 originated from a past stripping event of NGC 4579. They are both along the same direction from NGC 4579 and both have very similar radial velocities. This scenario would also be consistent with the observation that AGC 224219 has more H I gas than BC1, as the latter would have traveled twice as far from its parent object (∼150 Mpc, projected, in total). However, this scenario would not naturally explain why AGC 224219 appears to have an older, redder stellar population, while BC1 is dominated by young, blue stars (Figure 2) and H II regions. Furthermore, if a large quantity of gas had been stripped from NGC 4579 in the recent past then its H I and CO distributions would probably show more signs of disturbance and other clumps of in situ SF would be expected in the immediate vicinity.

The discussion above exhausts the possible sources of gas, within 1° (∼300 kpc) and ±500 km s^{-1}, from which BC1 could have formed. Assuming that we have not erroneously rejected the true source of the gas that formed BC1, we are left with three possibilities: a) the origin of the gas lies farther away than 1°, b) the gas originally belonged to a faint or LSB object that we have missed or excluded due to a lack of a redshift, or c) that BC1 was a (long-lived) dark object that contained gas but no stars prior to its recent SF episode.

Based on the simulations of Kapferer et al. (2009), neutral gas being ram pressure stripped can be found several hundred kiloparsecs from the source galaxy. However, increasing the search radius gives a large number of potential candidates owing to the density of the Virgo region. If we narrow these down to those that are blue or contain H I, and are very close in velocity to BC1 then VCC 1686 (IC 3583, $cz_\odot = 1122$ km s^{-1}, 71′ away), VCC 1992 (IC 3710, $cz_\odot = 1012$ km s^{-1}, 75′ away), AGC 225847 ($cz_\odot = 982$ km s^{-1}, 81′ away), and VCC 1931 ($cz_\odot = 1183$ km s^{-1}, 83′ away) are the most promising candidates (note that these are beyond the FoV shown in Figure 12). These are all irregular dwarf galaxies that appear to be forming stars and are likely interacting with other galaxies in the cluster.

VCC 1686 can be discounted as a foreground galaxy based on a TRGB distance measurement (Karachentsev et al. 2014). Estimating the stellar masses of the remaining three candidates (assuming $D = 16.5$ Mpc) with the mass-to-light ratio of Taylor et al. (2011) and photometry of Kim et al. (2014) and then applying the MZR of Andrews & Martini (2013) reveals that all have expected metallicities at least 0.2 dex lower than BC1 (Table 3). Thus we are left with no strong candidate that matches the properties of BC1.

B.2. BC4 & BC5

There are no galaxies with significant H I reservoirs (detectable in ALFALFA at the distance of Virgo) within 30′ and 500 km s^{-1} of BC4 (Figure 12, bottom left). However, the only (possible) Virgo member in the VCC or EVCC within 30′ is VCC 824 ($cz_\odot = 392$ km s^{-1}), a red ($g - i = 0.84$), nucleated, LSB dwarf. The nearest galaxy detected in H I is NGC 4419 (VCC 958, $cz_\odot = -275$ km s^{-1}), approximately 40′ to the north of BC4. The H I distribution of this galaxy has been greatly truncated (Chung et al. 2009), indicating that it has undergone significant ram pressure stripping. The VERTICO CO map of NGC 4419 (Brown et al. 2021) indicates that the molecular gas may extend roughly to the south. This could indicate that this galaxy has already fallen past the cluster center and is now moving to the north, in which case this could be a good candidate origin of the gas that formed BC4. The Taylor et al. (2011) relation for stellar mass (based on M_i and $g - i$) gives an estimate of $\log M_*/\mathrm{M}_\odot = 10.25 \pm 0.10$ for NGC 4419 (assuming $D = 16.5$ Mpc). Using this stellar mass estimate in the MZR of Andrews & Martini (2013) gives a metallicity estimate of $12 + \log(\mathrm{O/H}) = 8.74 \pm 0.18$, which matches remarkably well with the observed metallicity of the H II regions in BC4, $\langle 12 + \log(\mathrm{O/H})\rangle = 8.73 \pm 0.15$ (Section 4.2).

A little farther to the north there is another gas-bearing galaxy, NGC 4396 (VCC 865, $cz_\odot = -122$ km s^{-1}, 77′ away). This galaxy was also studied in the VIVA project, which found that it is in the process of being stripped by ram pressure. However, in this case the gas clearly extends to the NW, indicating that NGC 4396 is unlikely to be the source of the gas that formed BC4.

Skipping over a few low-mass H I detections (to which we shall return), the next nearest gas-bearing galaxies are to the south, NGC 4402 (VCC 873) and NGC 4438 (VCC 1043), both of which are ∼1.°3 from BC4 (beyond the FoV in Figure 12). NGC 4402 was imaged in H I by the VIVA survey, revealing that the galaxy is deficient in H I, exhibits a truncated disk and clear signs of ongoing ram pressure stripping, with the current gas tail emanating in a NW direction (Crowl et al. 2005). However, NGC 4402 has $cz_\odot = 230$ km s^{-1}, which places it ∼300 km s^{-1} away from BC4. Although this velocity separation does not rule out NGC 4402 as the origin of BC4, it means it is less favored than other candidates. NGC 4438 is just to the east of NGC 4402, and unfortunately does not have any existing H I imaging. However, the DECaLS images of NGC 4438 display a highly irregular morphology and the galaxy appears partially disrupted. The central velocity of the H I emission (Haynes et al. 2018) is $cz_\odot = 104$ km s^{-1}, placing it significantly closer to BC4 in velocity. Again using the Taylor et al. (2011) stellar mass-to-light relation and the photometry from the EVCC, these two galaxies have stellar mass estimates of $\log M_*/\mathrm{M}_\odot = 9.98 \pm 0.10$ and 10.57 ± 0.10, respectively. Thus neither would match with the metallicity of BC4 (via the MZR) quite as well as NGC 4419, but would agree comfortably within the relation's scatter.

We also note that BC4 is in the vicinity of SECCO 1 and Sand et al. (2017) suggested the same subgroup of Virgo (containing NGC 4402 and NGC 4438) as the potential source of the gas in that object. The extension of NGC 4402 to the NW (Crowl et al. 2005; Chung et al. 2009) and the highly disturbed Hα emission (Kenney et al. 2008; Sand et al. 2017) in the vicinity of both galaxies makes them both plausible candidates for the origin of SECCO 1. However, this does not preclude them also being candidates for BC4. It is possible that several such objects may be formed from the ram pressure stripping of a single large galaxy, but the significantly lower metallicity of SECCO 1 (though still high for such a low-mass object, $12 + \log(\mathrm{O/H}) = 8.38$; Beccari et al. 2017a) suggests that it was likely formed from a different parent object than BC4.

Finally, we return to the two blue, irregular, dwarf galaxies to the south of BC4 that we skipped over above, VCC 1001

($cz_{\odot} = 340$ km s^{-1}, 43′ away) and VCC 945 (IC 3355, $cz_{\odot} = -16$ km s^{-1}, 73′ away). These are likely too small and far away from BC4 to have been the source of the gas it must have had recently to support its SF. However, they may be related to BC4, or indeed to NGC 4402 and NGC 4438. It is also worth noting that three very similar objects were seen in the vicinity of BC1 on the other side of the cluster.

BC5 is approximately 45′ north of BC4, raising the possibility that perhaps it is part of the same extended structure, indeed the two objects have almost identical metallicity measurements (Table 3) and radial velocities (Table 1). The closest galaxy detected in H I (and within 500 km s^{-1}) is NGC 4419 (VCC 958, ∼10′ to the SE), as it was for BC4 (Figure 12, bottom right). Again this object would be an excellent match for BC5's metallicity (based on the MZR). However, if we assume these objects formed from ram pressured stripped material then it seems unlikely that NGC 4419 could be the origin of both BC4 and BC5, as BC4 is 40′ to its south and BC5 is 10′ to its NW, while ram pressure tails usually extend in one general direction (i.e., in the wake of the galaxy's motion through the ICM). If instead they were formed from tidally stripped gas then this objection is removed, as they may have formed from tidal tails on opposite sides of the galaxy.

The next nearest galaxy is NGC 4396, 30′to the NW. As discussed above, this galaxy is also being stripped; however, as with BC4, the H I tail extends in the wrong direction.

These two galaxies are the only H I-bearing galaxies within 1° and ±500 km s^{-1}. The only other galaxy in the VCC or EVCC within this range is VCC 583, a red, LSB dwarf elliptical approximately 58′ to the west. This dwarf is next to the H I-bearing galaxy NGC 4312, which might have been a good candidate for the origin of both BC4 and BC5 via ram pressure stripping, except that multiple TFR distance estimates place it well in the foreground of the cluster (Yasuda et al. 1997; Russell 2002; Sorce et al. 2014).

Thus if we wish to look for better-matched candidates then we must look further afield. Here we come across a promising candidate, UGC 7695 (VCC 1450, IC 3476; $cz_{\odot} = -159$ km s^{-1}, ∼1°.5 to the SE of BC4, beyond the FoV shown in Figure 12). This galaxy was extensively studied by Boselli et al. (2021). It displays a striking bow-shaped region bright in Hα and UV, a clear sign of ram pressure stripping. Boselli et al. (2021) argue that this galaxy is likely being stripped almost edge-on and that the stripped gas is forced up, over and around the disk. The metallicity of UGC 7695 is also consistent with that of BC4 and BC5, with the highest values measured by Boselli et al. (2021) being $12 + \log(\mathrm{O/H}) \approx 8.7$ and the average being $\langle 12 + \log(\mathrm{O/H}) \rangle = 8.60 \pm 0.12$ (Hughes et al. 2013).

The orientation of UGC 7695 and its velocity relative to the cluster center suggest that the transverse velocity through the cluster is likely on the order of 1500 km s^{-1} (Boselli et al. 2021). Based on this velocity, the material that formed BC4 and BC5 would have needed to have been stripped approximately 250–300 Myr ago. This is consistent with the approximate ages of the stellar populations of the BCs that we estimated in Section 4.4, in that those age estimates are less (∼200 Myr). But, Boselli et al. (2021) conclude that the structures seen in UGC 7695are considerably younger, 50–150 Myr. However, their simulations of the stripping of UGC 7695 assume constant properties for the ICM, whereas if it has traversed over 450 kpc through the cluster, then the surrounding density will have changed significantly during the course of its interaction. It is also possible that the gas that formed BC4 and BC5 was the first material to be stripped, before the ram pressure was sufficient to strip the main disk. We note that the metallicities of BC4 and BC5 correspond to the most metal-rich measurements of UGC 7695. This may be an indication that their seed gas originated in a particularly metal-rich region, such as gas that has been enriched by recent supernovae and pushed far from the plane of the galaxy. We therefore suggest that despite the young age estimate of the ram pressure stripping event in Boselli et al. (2021), UGC 7695 is still consistent with being the origin of these two BCs.

Finally, we note that in the ALFALFA data cube the H I emission appears to extend slightly from UGC 7695 in the approximate direction of BC4 and BC5, but unfortunately this emission cannot be reliably traced as it becomes blended with Galactic H I emission at the same velocity. Given the morphology, orientation, and location of UGC 7695, along with its estimated metallicity, this is by far the best candidate for the origin of that material that formed BC4 and BC5.

ORCID iDs

Michael G. Jones https://orcid.org/0000-0002-5434-4904
David J. Sand https://orcid.org/0000-0003-4102-380X
Michele Bellazzini https://orcid.org/0000-0001-8200-810X
Kristine Spekkens https://orcid.org/0000-0002-0956-7949
Ananthan Karunakaran https://orcid.org/0000-0001-8855-3635
Elizabeth A. K. Adams https://orcid.org/0000-0002-9798-5111
Giuseppina Battaglia https://orcid.org/0000-0002-6551-4294
Giacomo Beccari https://orcid.org/0000-0002-3865-9906
Paul Bennet https://orcid.org/0000-0001-8354-7279
John M. Cannon https://orcid.org/0000-0002-1821-7019
Giovanni Cresci https://orcid.org/0000-0002-5281-1417
Denija Crnojević https://orcid.org/0000-0002-1763-4128
Nelson Caldwell https://orcid.org/0000-0003-2352-3202
Jackson Fuson https://orcid.org/0000-0002-8598-439X
Puragra Guhathakurta https://orcid.org/0000-0001-8867-4234
Martha P. Haynes https://orcid.org/0000-0001-5334-5166
John L. Inoue https://orcid.org/0000-0002-9724-8998
Laura Magrini https://orcid.org/0000-0003-4486-6802
Ricardo R. Muñoz https://orcid.org/0000-0002-0810-5558
Burçin Mutlu-Pakdil https://orcid.org/0000-0001-9649-4815
Anil Seth https://orcid.org/0000-0003-0248-5470
Jay Strader https://orcid.org/0000-0002-1468-9668
Elisa Toloba https://orcid.org/0000-0001-6443-5570
Dennis Zaritsky https://orcid.org/0000-0002-5177-727X

References

Adams, E. A. K., Cannon, J. M., Rhode, K. L., et al. 2015, A&A, 580, A134
Adams, E. A. K., Giovanelli, R., & Haynes, M. P. 2013, ApJ, 768, 77
Adams, E. A. K., Oosterloo, T. A., Cannon, J. M., Giovanelli, R., & Haynes, M. P. 2016, A&A, 596, A117
Andrews, B. H., & Martini, P. 2013, ApJ, 765, 140
Asplund, M., Grevesse, N., Sauval, A. J., & Scott, P. 2009, ARA&A, 47, 481
Bacon, R., Vernet, J., Borisova, E., et al. 2014, Msngr, 157, 13
Beccari, G., Bellazzini, M., Magrini, L., et al. 2017a, MNRAS, 465, 2189
Beccari, G., Bellazzini, M., Magrini, L., et al. 2017b, MNRAS, 468, 4254

Bellazzini, M., Armillotta, L., Perina, S., et al. 2018, MNRAS, 476, 4565
Bellazzini, M., Magrini, L., Jones, M. G., et al. 2022, ApJ, in press, arXiv:2206.13971
Bellazzini, M., Magrini, L., Mucciarelli, A., et al. 2015, ApJL, 800, L15
Berg, D. A., Skillman, E. D., Marble, A. R., et al. 2012, ApJ, 754, 98
Beroiz, M., Cabral, J., & Sanchez, B. 2020, A&C, 32, 100384
Bertin, E., & Arnouts, S. 1996, A&AS, 117, 393
Binggeli, B., Sandage, A., & Tammann, G. A. 1985, AJ, 90, 1681
Boch, T., & Fernique, P. 2014, in ASP Conf. Ser. 485, Astronomical Data Analysis Software and Systems XXIII, ed. N. Manset & P. Forshay (San Francisco, CA: ASP), 277
Bolatto, A. D., Wolfire, M., & Leroy, A. K. 2013, ARA&A, 51, 207
Bonnarel, F., Fernique, P., Bienaymé, O., et al. 2000, A&AS, 143, 33
Boselli, A., Boissier, S., Heinis, S., et al. 2011, A&A, 528, A107
Boselli, A., Fossati, M., Ferrarese, L., et al. 2018, A&A, 614, A56
Boselli, A., Fossati, M., & Sun, M. 2022, A&ARv, 30, 3
Boselli, A., Lupi, A., Epinat, B., et al. 2021, A&A, 646, A139
Bournaud, F., & Duc, P. A. 2006, A&A, 456, 481
Bradley, L., Sipőcz, B., Robitaille, T., et al. 2020, astropy/photutils: v1.0.0, v1.0.0, Zenodo, doi:10.5281/zenodo.4044744
Bressan, A., Marigo, P., Girardi, L., et al. 2012, MNRAS, 427, 127
Brown, T., Wilson, C. D., Zabel, N., et al. 2021, ApJS, 257, 21
Calura, F., Bellazzini, M., & D'Ercole, A. 2020, MNRAS, 499, 5873
Canning, R. E. A., Ryon, J. E., Gallagher, J. S., et al. 2014, MNRAS, 444, 336
Cannon, J. M., Martinkus, C. P., Leisman, L., et al. 2015, AJ, 149, 72
Chung, A., van Gorkom, J. H., Kenney, J. D. P., Crowl, H., & Vollmer, B. 2009, AJ, 138, 1741
Conselice, C. J., Gallagher, J. S. I., & Wyse, R. F. G. 2001, AJ, 122, 2281
Corbelli, E., Cresci, G., Mannucci, F., Thilker, D., & Venturi, G. 2021, ApJL, 908, L39
Cortese, L., Catinella, B., & Smith, R. 2021, PASA, 38, e035
Cortese, L., Marcillac, D., Richard, J., et al. 2007, MNRAS, 376, 157
Crowl, H. H., Kenney, J. D. P., van Gorkom, J. H., & Vollmer, B. 2005, AJ, 130, 65
Croxall, K. V., van Zee, L., Lee, H., et al. 2009, ApJ, 705, 723
Davies, J. I., Davies, L. J. M., & Keenan, O. C. 2016, MNRAS, 456, 1607
De Vis, P., Jones, A., Viaene, S., et al. 2019, A&A, 623, A5
Dolphin, A. 2016, DOLPHOT: Stellar photometry, Astrophysics Source Code Library, ascl:1608.013
Dolphin, A. E. 2000, PASP, 112, 1383
Duc, P. A., Braine, J., Lisenfeld, U., Brinks, E., & Boquien, M. 2007, A&A, 475, 187
Duc, P. A., & Mirabel, I. F. 1998, A&A, 333, 813
Eckert, D., Roncarelli, M., Ettori, S., et al. 2015, MNRAS, 447, 2198
Ferrarese, L., Côté, P., Cuillandre, J.-C., et al. 2012, ApJS, 200, 4
Fumagalli, M., Gavazzi, G., Scaramella, R., & Franzetti, P. 2011, A&A, 528, A46
Giovanelli, R., Haynes, M. P., Adams, E. A. K., et al. 2013, AJ, 146, 15
Giovanelli, R., Haynes, M. P., Kent, B. R., et al. 2005, AJ, 130, 2598
Green, G. M. 2018, JOSS, 3, 695
Haynes, M. P., & Giovanelli, R. 1984, AJ, 89, 758
Haynes, M. P., Giovanelli, R., Kent, B. R., et al. 2018, ApJ, 861, 49
Haynes, M. P., Giovanelli, R., Martin, A. M., et al. 2011, AJ, 142, 170
Hester, J. A., Seibert, M., Neill, J. D., et al. 2010, ApJL, 716, L14
Hirschauer, A. S., Salzer, J. J., Skillman, E. D., et al. 2016, ApJ, 822, 108
Hsyu, T., Cooke, R. J., Prochaska, J. X., & Bolte, M. 2017, ApJL, 845, L22
Huang, S., Haynes, M. P., Giovanelli, R., & Brinchmann, J. 2012, ApJ, 756, 113
Hughes, T. M., Cortese, L., Boselli, A., Gavazzi, G., & Davies, J. I. 2013, A&A, 550, A115
Iglesias-Páramo, J., Buat, V., Takeuchi, T. T., et al. 2006, ApJS, 164, 38
Irwin, M. J., Belokurov, V., Evans, N. W., et al. 2007, ApJL, 656, L13
Izotov, Y. I., Thuan, T. X., & Guseva, N. G. 2019, MNRAS, 483, 5491
Jáchym, P., Kenney, J. D. P., Sun, M., et al. 2019, ApJ, 883, 145
Jaffé, Y. L., Poggianti, B. M., Moretti, A., et al. 2018, MNRAS, 476, 4753
James, B. L., Koposov, S., Stark, D. P., et al. 2015, MNRAS, 448, 2687
Janesh, W., Rhode, K. L., Salzer, J. J., et al. 2019, AJ, 157, 183
Jiang, F., Dekel, A., Freundlich, J., et al. 2019, MNRAS, 487, 5272
Jones, M. G., Sand, D. J., Bellazzini, M., et al. 2022, ApJL, 926, L15
Joye, W. A., & Mandel, E. 2003, in ASP Conf. Ser. 295, Astronomical Data Analysis Software and Systems XII, ed. H. E. Payne, R. I. Jedrzejewski, & R. N. Hook (San Francisco, CA: ASP), 489
Junais, Boissier, S., Boselli, A., et al. 2021, A&A, 650, A99
Kapferer, W., Sluka, C., Schindler, S., Ferrari, C., & Ziegler, B. 2009, A&A, 499, 87
Karachentsev, I. D., Tully, R. B., Wu, P.-F., Shaya, E. J., & Dolphin, A. E. 2014, ApJ, 782, 4
Kashibadze, O. G., Karachentsev, I. D., & Karachentseva, V. E. 2020, A&A, 635, A135
Kenney, J. D. P., Geha, M., Jáchym, P., et al. 2014, ApJ, 780, 119
Kenney, J. D. P., Tal, T., Crowl, H. H., Feldmeier, J., & Jacoby, G. H. 2008, ApJL, 687, L69
Kennicutt, R. C. J. 1998, ARA&A, 36, 189
Kennicutt, R. C. J., Lee, J. C., Funes, J. G., et al. 2008, ApJS, 178, 247
Kent, B. R., Spekkens, K., Giovanelli, R., et al. 2009, ApJ, 691, 1595
Kim, S., Rey, S.-C., Jerjen, H., et al. 2014, ApJS, 215, 22
Kirby, E. N., Cohen, J. G., Guhathakurta, P., et al. 2013, ApJ, 779, 102
Kleiner, D., Serra, P., Maccagni, F. M., et al. 2021, A&A, 648, A32
Kronberger, T., Kapferer, W., Ferrari, C., Unterguggenberger, S., & Schindler, S. 2008, A&A, 481, 337
Lee, J., Kimm, T., Blaizot, J., et al. 2022, ApJ, 928, 144
Lee, J. C., Gil de Paz, A., Tremonti, C., et al. 2009, ApJ, 706, 599
Lee-Waddell, K., Madrid, J. P., Spekkens, K., et al. 2018, MNRAS, 480, 2719
Licquia, T. C., & Newman, J. A. 2015, ApJ, 806, 96
Lim, P. L., Davis, M., Hack, W., et al. 2020, ACStools: Python tools for Hubble Space Telescope Advanced Camera for Surveys data, Astrophysics Source Code Library, ascl:2011.024
Martin, D. C., Fanson, J., Schiminovich, D., et al. 2005, ApJL, 619, L1
McMullin, J. P., Waters, B., Schiebel, D., Young, W., & Golap, K. 2007, in ASP Conf. Ser. 376, Astronomical Data Analysis Software and Systems XVI, ed. R. A. Shaw, F. Hill, & D. J. Bell (San Francisco, CA: ASP), 127
McQuinn, K. B. W., Berg, D. A., Skillman, E. D., et al. 2020, ApJ, 891, 181
McQuinn, K. B. W., Skillman, E. D., Dalcanton, J. J., et al. 2011, ApJ, 740, 48
McQuinn, K. B. W., Skillman, E. D., Dolphin, A., et al. 2015b, ApJ, 812, 158
McQuinn, K. B. W., Skillman, E. D., Dolphin, A. E., & Mitchell, N. P. 2015a, ApJ, 808, 109
Mei, S., Blakeslee, J. P., Côté, P., et al. 2007, ApJ, 655, 144
Mendes de Oliveira, C., Cypriano, E. S., Sodré, L., & Balkowski, C, J. 2004, ApJL, 605, L17
Minchin, R. F., Taylor, R., Köppen, J., et al. 2019, AJ, 158, 121
Morandi, A., & Cui, W. 2014, MNRAS, 437, 1909
Moretti, A., Paladino, R., Poggianti, B. M., et al. 2018, MNRAS, 480, 2508
Moretti, A., Paladino, R., Poggianti, B. M., et al. 2020, ApJ, 889, 9
Morrissey, P., Conrow, T., Barlow, T. A., et al. 2007, ApJS, 173, 682
Müller, A., Ignesti, A., Poggianti, B., et al. 2021, Galax, 9, 116
Muñoz, R. P., Eigenthaler, P., Puzia, T. H., et al. 2015, ApJL, 813, L15
Nulsen, P. E. J., & Bohringer, H. 1995, MNRAS, 274, 1093
Oman, K. A., Bahé, Y. M., Healy, J., et al. 2021, MNRAS, 501, 5073
Oman, K. A., & Hudson, M. J. 2016, MNRAS, 463, 3083
Peletier, R., Iodice, E., Venhola, A., et al. 2020, arXiv:2008.12633
Pettini, M., & Pagel, B. E. J. 2004, MNRAS, 348, L59
Poggianti, B. M., Gullieuszik, M., Tonnesen, S., et al. 2019, MNRAS, 482, 4466
Astropy Collaboration, Price-Whelan, A. M., Sipőcz, B. M., et al. 2018, AJ, 156, 123
Querejeta, M., Lelli, F., Schinnerer, E., et al. 2021, A&A, 645, A97
Robitaille, T. 2019, APLpy v2.0: The Astronomical Plotting Library in Python, v2.0, Zenodo, doi:10.5281/zenodo.2567476
Robitaille, T., & Bressert, E. 2012, APLpy: Astronomical Plotting Library in Python, Astrophysics Source Code Library, ascl:1208.017
Robitaille, T., Deil, C., & Ginsburg, A. 2020, Reproject: Python-based astronomical image reprojection, Astrophysics Source Code Library, ascl:2011.023
Astropy Collaboration, Robitaille, T. P., Tollerud, E. J., et al. 2013, A&A, 558, A33
Russell, D. G. 2002, ApJ, 565, 681
Sand, D. J., Crnojević, D., Bennet, P., et al. 2015, ApJ, 806, 95
Sand, D. J., Seth, A. C., Crnojević, D., et al. 2017, ApJ, 843, 134
Saul, D. R., Peek, J. E. G., Grcevich, J., et al. 2012, ApJ, 758, 44
Schlafly, E. F., & Finkbeiner, D. P. 2011, ApJ, 737, 103
Schlegel, D. J., Finkbeiner, D. P., & Davis, M. 1998, ApJ, 500, 525
Scott, T. C., Cortese, L., Lagos, P., et al. 2022, MNRAS, 511, 980
Serra, P., de Blok, W. J. G., Bryan, G. L., et al. 2016, in Proc. of MeerKAT Science: On the Pathway to the SKA, https://pos.sissa.it/cgi-bin/reader/conf.cgi?confid=277
Sijacki, D., Vogelsberger, M., Kereš, D., Springel, V., & Hernquist, L. 2012, MNRAS, 424, 2999
Skillman, E. D., Salzer, J. J., Berg, D. A., et al. 2013, AJ, 146, 3
Smith, R., Davies, J. I., & Nelson, A. H. 2010, MNRAS, 405, 1723
Sorce, J. G., Tully, R. B., Courtois, H. M., et al. 2014, MNRAS, 444, 527

Sun, M., Donahue, M., & Voit, G. M. 2007, ApJ, 671, 190
Sun, M., Ge, C., Luo, R., et al. 2021, NatAs, 6, 270
Taylor, E. N., Hopkins, A. M., Baldry, I. K., et al. 2011, MNRAS, 418, 1587
Taylor, R., Davies, J. I., Auld, R., Minchin, R. F., & Smith, R. 2013, MNRAS, 428, 459
Tonnesen, S., & Bryan, G. L. 2012a, MNRAS, 422, 1609
Tonnesen, S., & Bryan, G. L. 2012b, MNRAS, 422, 1609
Tonnesen, S., & Bryan, G. L. 2021, ApJ, 911, 68
Vollmer, B., Cayatte, V., Balkowski, C., & Duschl, W. J. 2001, ApJ, 561, 708
Weilbacher, P. M., Duc, P. A., & Fritze-v. Alvensleben, U. 2003, A&A, 397, 545
Weisz, D. R., Dolphin, A. E., Skillman, E. D., et al. 2014, ApJ, 789, 147
Wyder, T. K., Martin, D. C., Schiminovich, D., et al. 2007, ApJS, 173, 293
Yasuda, N., Fukugita, M., & Okamura, S. 1997, ApJS, 108, 417
Yoshida, M., Yagi, M., Komiyama, Y., et al. 2008, ApJ, 688, 918
Zibetti, S., Charlot, S., & Rix, H.-W. 2009, MNRAS, 400, 1181